A low-order nonconforming method for linear elasticity on general meshes

Michele Botti, Daniele Antonio Di Pietro, Alessandra Guglielmana

A low-order nonconforming method for linear elasticity on general meshes*

Michele Botti[a], Daniele A. Di Pietro[a] and Alessandra Guglielmana[a,b]

[a]IMAG, Univ Montpellier, CNRS, Montpellier, France
[b]Politecnico di Milano, 20133 Milano, Italy

ARTICLE INFO

Keywords:
Linear elasticity
Korn's inequality
locking-free methods
Hybrid High-Order methods
polyhedral meshes

ABSTRACT

In this work we construct a low-order nonconforming approximation method for linear elasticity problems supporting general meshes and valid in two and three space dimensions. The method is obtained by hacking the Hybrid High-Order method of Di Pietro and Ern (2015), that requires the use of polynomials of degree $k \geq 1$ for stability. Specifically, we show that coercivity can be recovered for $k = 0$ by introducing a novel term that penalises the jumps of the displacement reconstruction across mesh faces. This term plays a key role in the fulfillment of a discrete Korn inequality on broken polynomial spaces, for which a novel proof valid for general polyhedral meshes is provided. Locking-free error estimates are derived for both the energy- and the L^2-norms of the error, that are shown to convergence, for smooth solutions, as h and h^2, respectively (here, h denotes the meshsize). A thorough numerical validation on a complete panel of two- and three-dimensional test cases is provided.

1. Introduction

Discretisation methods supporting meshes with general, possibly non standard, element shapes have experienced a vigorous growth over the last few years. In the context of solid-mechanics, this feature can be useful for several reasons including, e.g., improved robustness to mesh distortion and fracture, local mesh refinement, or the use of hanging nodes for contact and interface problems. A non-exahustive list of contributions in the context of elasticity problems includes Hughes, Cottrell and Bazilevs (2005); Tabarraei and Sukumar (2006); Beirão Da Veiga (2010); Beirão da Veiga, Brezzi and Marini (2013); Droniou and Lamichhane (2015); Gain, Talischi and Paulino (2014); Di Pietro and Lemaire (2015); Di Pietro and Ern (2015); Wriggers, Rust and Reddy (2016); Botti, Di Pietro and Sochala (2017); Artioli, Beirão da Veiga, Lovadina and Sacco (2017); Koyama and Kikuchi (2017); Cockburn and Fu (2018); Sevilla, Giacomini, Karkoulias and Huerta (2018); Cáceres, Gatica and Sequeira (2019); see also references therein.

For large three-dimensional simulations, or whenever one cannot expect the exact solution to be smooth, low-order methods are often privileged in order to reduce the number of unknowns. It is well-known, however, that low-order Finite Element (FE) approximations are in some cases unsatisfactory: affine conforming FE methods are not robust in the quasi-incompressible limit owing to their inability to represent non-trivial divergence-free displacement fields; nonconforming (Crouzeix–Raviart) FE methods, on the other hand, yield unstable discretisations unless appropriate measures are taken; see, e.g., the discussions in Brenner and Sung (1992); Hansbo and Larson (2003). The underlying reason for this lack of stability is the non-fulfillment of a discrete counterpart of Korn's inequality owing to a poor control of rigid-body motions at mesh faces. For similar reasons, the stability of Hybrid High-Order (HHO) methods for linear elasticity requires the use of polynomials of degree $k \geq 1$ as unknowns; see (Di Pietro and Ern, 2015, Lemma 4). As a matter of fact, as we show in Section 4.4 below, the stability and consistency requirements on the local HHO stabilisation term are incompatible when $k = 0$, that is, when piecewise constant polynomials on the mesh and its skeleton are used as discrete unknowns.

In this paper we highlight a modification of the HHO method which recovers stability for $k = 0$. The proposed fix consists in adding a novel term which penalises in a least square sense the jumps of the local affine displacement

*The work of the second author was partially supported by *Agence Nationale de la Recherche* grants HHOMM (ANR-15-CE40-0005) and fast4hho (ANR-17-CE23-0019).

bottieaffini@gmail.com (M. Botti); daniele.di-pietro@umontpellier.fr (D.A. Di Pietro); alessandra.guglielmana@mail.polimi.it (A. Guglielmana)
https://imag.umontpellier.fr/~di-pietro/ (D.A. Di Pietro)
ORCID(s): 0000-0003-0959-8830 (D.A. Di Pietro)

reconstruction. This modification is inspired by the Korn inequality on broken polynomial spaces proved in Lemma 1 below, which appears to be a novel extension of similar results to general polyhedral meshes. The proof combines the techniques of (Brenner, 2003, Lemma 2.2) with the recent results of Di Pietro and Ern (2012) and Di Pietro and Droniou (2017a) concerning, respectively, the node-averaging operator and local inverse inequalities on polyhedral meshes. In the context of Crouzeix–Raviart FE approximations of linear elasticity problems on standard meshes, similar jump penalisation terms have been considered in Hansbo and Larson (2003).

The resulting method has several appealing features: it is valid in two and three space dimensions, paving the way to unified implementations; it hinges on a reduced number of unknowns (15 for a tetrahedron, 21 for a hexahedron and, for more general polyhedral shapes, 3 unknowns per face plus 3 unknowns inside the element); it is robust in the quasi-incompressible limit; it admits a formulation in terms of conservative numerical tractions, which enables its integration in existing Finite Volume simulators (a particularly relevant feature in the context of industrial applications).

We carry out a complete convergence analysis based on the abstract framework of Di Pietro and Droniou (2018) for methods in fully discrete formulation. Specifically, we show that the energy and L^2-norms of the error converge, respectively, as h and h^2 (with h denoting, as usual, the meshsize). As for the original HHO method of Di Pietro and Ern (2015), the error estimates are additionally shown to be robust in the quasi-incompressible limit. Key to this result is the fact that the gradient of the local displacement reconstruction satisfies a suitable commutation property with the L^2-orthogonal projector. The theoretical results are supported by a thorough numerical investigation, including two- and three-dimensional test cases, as well as a comparison with the original HHO method of Di Pietro and Ern (2015) on a test case mimicking a mode 1 fracture.

The rest of the paper is organised as follows. In Section 2 we formulate the continuous problem along with the assumptions on the problem data. In Section 3 we establish the discrete setting: after briefly recalling the notion of regular polyhedral mesh, we introduce local and broken polynomial spaces and projectors thereon, and we prove a discrete counterpart of Korn's first inequality on broken polynomial spaces. In Section 4 we introduce the space of discrete unknowns, define a local affine displacement reconstruction, formulate the discrete bilinear form, discuss the differences with respect to the original HHO bilinear form of Di Pietro and Ern (2015), and state the discrete problem. Section 5 addresses the convergence analysis of the method in the energy- and L^2-norms, while Section 6 contains an exhaustive panel of two- and three-dimensional numerical tests. Finally, in Section 7 we show that the method satisfies local balances with equilibrated tractions, for which an explicit expression is provided.

2. Continuous setting

Consider a body which, in its reference configuration, occupies a given region of space $\Omega \subset \mathbb{R}^d$, $d \in \{2,3\}$. In what follows, it is assumed that Ω is a bounded connected open polygonal (if $d = 2$) or polyhedral (if $d = 3$) set that does not have cracks, i.e., it lies on one side of its boundary $\partial\Omega$. We are interested in finding the displacement field $\boldsymbol{u} : \Omega \to \mathbb{R}^d$ of the body when it is subjected to a given force per unit volume $\boldsymbol{f} : \Omega \to \mathbb{R}^d$. We work in what follows under the small deformation assumption which implies, in particular, that the strain tensor $\boldsymbol{\varepsilon}$ is given by the symmetric part of the gradient of the displacement field, i.e., $\boldsymbol{\varepsilon} = \boldsymbol{\nabla}_{\mathrm{s}}\boldsymbol{u}$ where, for any vector-valued function $\boldsymbol{z} = (z_i)_{1\le i\le d}$ smooth enough, we have set $\boldsymbol{\nabla}\boldsymbol{z} = (\partial_j z_i)_{1\le i,j\le d}$ and $\boldsymbol{\nabla}_{\mathrm{s}}\boldsymbol{z} \coloneqq \frac{1}{2}\left(\boldsymbol{\nabla}\boldsymbol{z} + \boldsymbol{\nabla}\boldsymbol{z}^{\mathsf{T}}\right)$. We further assume, for the sake of simplicity, that the body is clamped along its boundary $\partial\Omega$. Other standard boundary conditions can be considered up to minor modifications. The displacement field is obtained by solving the following linear elasticity problem, which expresses the equilibrium between internal stresses and external loads: Find $\boldsymbol{u} : \Omega \to \mathbb{R}^d$ such that

$$-\boldsymbol{\nabla}\cdot(\boldsymbol{\sigma}(\boldsymbol{\nabla}_{\mathrm{s}}\boldsymbol{u})) = \boldsymbol{f} \qquad \text{in } \Omega, \tag{1a}$$

$$\boldsymbol{u} = \boldsymbol{0} \qquad \text{on } \partial\Omega, \tag{1b}$$

where, denoting by $\mathbb{R}^{d\times d}_{\mathrm{sym}}$ the set of symmetric real-valued $d \times d$ matrices, the mapping $\boldsymbol{\sigma} : \mathbb{R}^{d\times d}_{\mathrm{sym}} \to \mathbb{R}^{d\times d}_{\mathrm{sym}}$ represents the strain-stress law. For isotropic homogeneous materials, the strain-stress law is such that, for any $\boldsymbol{\tau} \in \mathbb{R}^{d\times d}_{\mathrm{sym}}$,

$$\boldsymbol{\sigma}(\boldsymbol{\tau}) = 2\mu\boldsymbol{\tau} + \lambda\,\mathrm{tr}(\boldsymbol{\tau})\boldsymbol{I}_d, \tag{2}$$

where $\mathrm{tr}(\boldsymbol{\tau}) \coloneqq \sum_{i=1}^d \tau_{ii}$ is the trace operator and $\boldsymbol{I}_d$ the $d \times d$ identity matrix. The real numbers μ and λ, which correspond to the Lamé coefficients when $d = 3$, are assumed such that, for a real number $\alpha > 0$,

$$2\mu - d\lambda^- \ge \alpha, \tag{3}$$

where $\lambda^- \coloneqq \frac{1}{2}(|\lambda| - \lambda)$ denotes the negative part of λ. In what follows, μ, λ, the related bound (3), and $\boldsymbol{f}$ will be collectively referred to as the problem data.

For any open bounded set $X \subset \Omega$, we denote by $(\cdot,\cdot)_X$ the usual inner product of the space of scalar-valued, square-integrable functions $L^2(X;\mathbb{R})$, by $\|\cdot\|_X$ the corresponding norm, and we adopt the convention that the subscript is omitted whenever $X = \Omega$. The same notation is used for the spaces of vector- and tensor-valued square-integrable functions $L^2(X;\mathbb{R}^d)$ and $L^2(X;\mathbb{R}^{d\times d})$, respectively. With this notation, a classical weak formulation of problem (1) reads: Find $\boldsymbol{u} \in H^1_0(\Omega;\mathbb{R}^d)$ such that

$$(\boldsymbol{\sigma}(\boldsymbol{\nabla}_s\boldsymbol{u}), \boldsymbol{\nabla}_s\boldsymbol{v}) = (\boldsymbol{f},\boldsymbol{v}) \qquad \forall \boldsymbol{v} \in H^1_0(\Omega;\mathbb{R}^d), \tag{4}$$

where $H^1_0(\Omega;\mathbb{R}^d)$ classically denotes the space of vector-valued functions that are square-integrable along with all their partial derivatives, and whose traces on $\partial\Omega$ vanish.

3. Discrete setting

3.1. Mesh

Throughout the rest of the paper, we will use for the sake of simplicity the three-dimensional nomenclature also when $d = 2$, i.e., we will speak of polyhedra and faces rather than polygons and edges. We consider here meshes corresponding to couples $\mathcal{M}_h \coloneqq (\mathcal{T}_h, \mathcal{F}_h)$, where $\mathcal{T}_h$ is a finite collection of polyhedral elements T such that $h \coloneqq \max_{T\in\mathcal{T}_h} h_T > 0$ with h_T denoting the diameter of T, while $\mathcal{F}_h$ is a finite collection of planar faces F. It is assumed henceforth that the mesh $\mathcal{M}_h$ matches the geometrical requirements detailed in (Droniou, Eymard, Gallouët, Guichard and Herbin, 2018, Definition 7.2); see also (Di Pietro and Tittarelli, 2018, Section 2). This covers, essentially, any reasonable partition of Ω into polyhedral sets, not necessarily convex or even star-shaped. For every mesh element $T \in \mathcal{T}_h$, we denote by $\mathcal{F}_T$ the subset of $\mathcal{F}_h$ containing the faces that lie on the boundary ∂T of T. Symmetrically, for every face $F \in \mathcal{F}_h$, we denote by $\mathcal{T}_F$ the subset of $\mathcal{T}_h$ containing the (one or two) mesh elements that share F. For any mesh element $T \in \mathcal{T}_h$ and each face $F \in \mathcal{F}_T$, $\boldsymbol{n}_{TF}$ is the constant unit normal vector to F pointing out of T. Boundary faces lying on $\partial\Omega$ and internal faces contained in Ω are collected in the sets $\mathcal{F}_h^{\mathrm{b}}$ and $\mathcal{F}_h^{\mathrm{i}}$, respectively. For any $F \in \mathcal{F}_h^{\mathrm{i}}$, we denote by T_1 and T_2 the elements of $\mathcal{T}_h$ such that $F \subset \partial T_1 \cap \partial T_2$. The numbering of T_1 and T_2 is assumed arbitrary but fixed, and we set $\boldsymbol{n}_F \coloneqq \boldsymbol{n}_{T_1F}$. Our focus is on the h-convergence analysis, so we consider a sequence of refined meshes that is regular in the sense of (Di Pietro and Tittarelli, 2018, Definition 4.3), that is, we assume the existence of a shape-regular matching simplicial submesh $\mathfrak{T}_h$ such that, for any $T \in \mathcal{T}_h$ and any $\tau \in \mathfrak{T}_h$ with $\tau \subset T$, the diameters of T and τ are comparable uniformly in h. This implies, in particular, that the diameter h_T of a mesh element $T \in \mathcal{T}_h$ is comparable to the diameter h_F of each face $F \in \mathcal{F}_T$ uniformly in h, and that the number of faces in $\mathcal{F}_T$ is bounded above by an integer N_∂ independent of h. Alternative assumptions covering degenerate faces can be found in Cangiani, Dong, Georgoulis and Houston (2017); see also references therein.

3.2. Local and broken spaces and projectors

In order to alleviate the exposition, throughout the rest of the paper we use the abridged notation $a \lesssim b$ for the inequality $a \le Cb$ with real number $C > 0$ independent of the meshsize, possibly on the problem data, and, for local inequalities, on the mesh element or face. We also write $a \simeq b$ for $a \lesssim b$ and $b \lesssim a$. The dependencies of the hidden constant are further specified whenever needed.

Let X denote a mesh element or face. For a given integer $l \ge 0$, we denote by $\mathbb{P}^l(X;\mathbb{R})$ the space spanned by the restriction to X of d-variate, real-valued polynomials of total degree $\le l$. The corresponding spaces of vector- and tensor-valued functions are respectively denoted by $\mathbb{P}^l(X;\mathbb{R}^d)$ and $\mathbb{P}^l(X;\mathbb{R}^{d\times d})$. A similar notation is used also for the vector and tensor versions of the broken spaces introduced in what follows. At the global level, we denote by $\mathbb{P}^l(\mathcal{T}_h;\mathbb{R})$ the space of broken polynomials on $\mathcal{T}_h$ whose restriction to every mesh element $T \in \mathcal{T}_h$ lies in $\mathbb{P}^l(T;\mathbb{R})$, i.e.,

$$\mathbb{P}^l(\mathcal{T}_h;\mathbb{R}) \coloneqq \left\{ v_h \in L^2(\Omega;\mathbb{R}) \ : \ v_{h|T} \in \mathbb{P}^l(T;\mathbb{R}) \quad \forall T \in \mathcal{T}_h \right\}.$$

We also introduce the broken Sobolev spaces

$$H^s(\mathcal{T}_h;\mathbb{R}) \coloneqq \left\{ v \in L^2(\Omega;\mathbb{R}) \ : \ v_{|T} \in H^s(T;\mathbb{R}) \quad \forall T \in \mathcal{T}_h \right\},$$

which will be used in the error estimates to express the regularity requirements on the exact solution. On $H^s(\mathcal{T}_h;\mathbb{R})$, we define the broken seminorm

$$|v|_{H^s(\mathcal{T}_h;\mathbb{R})} \coloneqq \left(\sum_{T\in\mathcal{T}_h} |v|^2_{H^s(T;\mathbb{R})}\right)^{\frac{1}{2}}.$$

Again denoting by X a mesh element or face, the local L^2-orthogonal projector $\pi^0_X : L^2(X;\mathbb{R}) \to \mathbb{P}^0(X;\mathbb{R})$ maps every $v \in L^2(X;\mathbb{R})$ onto the constant function equal to its mean value inside T, that is,

$$\pi^0_X v \coloneqq \frac{1}{|X|}\int_X v, \tag{5}$$

with $|X|$ denoting the Hausdorff measure of X. The vector and tensor versions of the L^2-projector, both denoted by $\boldsymbol{\pi}^0_X$, are obtained applying π^0_X component-wise. From (Di Pietro and Droniou, 2017a, Lemmas 3.4 and 3.6), it can be deduced that, for any mesh element $T \in \mathcal{T}_h$ and any function $v \in H^1(T;\mathbb{R})$, the following approximation properties hold:

$$\|v - \pi^0_T v\|_{L^2(T;\mathbb{R})} + h_T^{\frac{1}{2}}\|v - \pi^0_T v\|_{L^2(\partial T;\mathbb{R})} \lesssim h_T |v|_{H^1(T;\mathbb{R})}, \tag{6}$$

where ∂T denotes the boundary of T and the hidden constant is independent of h, T, and v. The global L^2-orthogonal projector $\pi^0_h : L^2(\Omega;\mathbb{R}) \to \mathbb{P}^0(\mathcal{T}_h;\mathbb{R})$ is such that, for any $v \in L^2(\Omega;\mathbb{R}^d)$,

$$(\pi^0_h v)_{|T} \coloneqq \pi^0_T v_{|T} \qquad \forall T \in \mathcal{T}_h. \tag{7}$$

The vector and tensor versions, both denoted by $\boldsymbol{\pi}^0_h$, are obtained applying π^0_h component-wise.

We will also need the elliptic projector $\varpi^1_T : H^1(T;\mathbb{R}) \to \mathbb{P}^1(T;\mathbb{R})$ such that, for all $v \in H^1(T;\mathbb{R})$,

$$\boldsymbol{\nabla}\varpi^1_T v = \boldsymbol{\pi}^0_T(\boldsymbol{\nabla} v) \text{ and } \frac{1}{|T|}\int_T \varpi^1_T v = \frac{1}{|T|}\int_T v. \tag{8}$$

The first relation makes sense since $\boldsymbol{\nabla}\mathbb{P}^1(T;\mathbb{R}) = \mathbb{P}^0(T;\mathbb{R}^d)$, and it defines $\varpi^1_T v$ up to a constant, which is then fixed by the second relation. Also in this case, the vector version $\boldsymbol{\varpi}^1_T$ of the projector is obtained applying the scalar version component-wise. The following approximation properties for the elliptic projector are a special case of (Di Pietro and Droniou, 2017b, Theorems 1.1 and 1.2): For all $T \in \mathcal{T}_h$ and all $v \in H^2(T;\mathbb{R})$,

$$\|v - \varpi^1_T v\|_{L^2(T;\mathbb{R})} + h_T^{\frac{1}{2}}\|v - \varpi^1_T v\|_{L^2(\partial T;\mathbb{R})} \lesssim h_T^2 |v|_{H^2(T;\mathbb{R})}, \tag{9}$$

where the hidden constant is independent of h, T, and v. For further use, we also define the global elliptic projector $\varpi^1_h : H^1(\mathcal{T}_h;\mathbb{R}) \to \mathbb{P}^1(\mathcal{T}_h;\mathbb{R})$ such that, for any $v \in H^1(\mathcal{T}_h;\mathbb{R})$,

$$(\varpi^1_h v)_{|T} \coloneqq \varpi^1_T v_{|T} \qquad \forall T \in \mathcal{T}_h.$$

The vector version $\boldsymbol{\varpi}^1_h$ of the global elliptic projector is obtained applying ϖ^1_h component-wise.

3.3. Discrete Korn inequality on broken polynomial spaces

The stability of our method hinges on a discrete counterpart of Korn's inequality in discrete polynomial spaces stating that the H^1-seminorm of a vector-valued broken polynomial function is controlled by a suitably defined strain norm. The goal of this section is to prove this inequality.

Let us start with some preliminary results. Recalling that, for any $F \in \mathcal{F}^{\mathrm{i}}_h$, we have denoted by T_1 and T_2 the elements sharing F and assumed that the ordering is arbitrary but fixed, we introduce the jump operator such that, for any function v smooth enough to admit a (possibly two-valued) trace on F,

$$[v]_F \coloneqq (v_{|T_1})_{|F} - (v_{|T_2})_{|F}. \tag{10a}$$

This operator is extended to boundary faces $F \in \mathcal{F}_h^{\mathrm{b}}$ by setting

$$[v]_F \coloneqq v_{|F}. \tag{10b}$$

When applied to vector-valued functions, the jump operator acts componentwise.

Let now $\mathfrak{T}_h$ denote a matching simplicial submesh of $\mathcal{M}_h$ in the sense of (Di Pietro and Tittarelli, 2018, Definition 4.2), and let $\mathfrak{F}_h$ be the corresponding set of simplicial faces. Given an integer $l \geq 1$, we define the node-averaging operator $I_{\mathrm{av},h}^l : \mathbb{P}^l(\mathcal{T}_h;\mathbb{R}) \to \mathbb{P}^l(\mathfrak{T}_h;\mathbb{R}) \cap H_0^1(\Omega)$ such that, for any function $v_h \in \mathbb{P}^l(\mathcal{T}_h;\mathbb{R})$ and any Lagrange node V of $\mathfrak{T}_h$, denoting by $\mathfrak{T}_V$ the set of simplices sharing V,

$$(I_{\mathrm{av},h}^l v_h)(V) \coloneqq \begin{cases} \dfrac{1}{\mathrm{card}(\mathfrak{T}_V)} \displaystyle\sum_{\tau \in \mathfrak{T}_V} (v_h)_{|\tau}(V) & \text{if } V \in \Omega, \\ 0 & \text{if } V \in \partial\Omega. \end{cases}$$

The vector-version, denoted by $\boldsymbol{I}_{\mathrm{av},h}^l$, acts component-wise. Adapting the reasoning of (Di Pietro and Ern, 2012, Section 5.5.2) (based in turn on Karakashian and Pascal (2003)), we infer that it holds, for all $T \in \mathcal{T}_h$,

$$\|v_h - I_{\mathrm{av},h}^l v_h\|_T^2 \lesssim \sum_{F \in \mathcal{F}_{\mathcal{V},T}} h_F \|[v_h]_F\|_F^2, \tag{11}$$

where $\mathcal{F}_{\mathcal{V},T}$ denotes the set of faces whose closure has nonempty intersection with the closure of T and the hidden constant is independent of h, T, and v_h. Combining this result with the inverse inequality of (Di Pietro and Droniou, 2017a, Remark A.2) (which remains valid for functions that are piecewise polynomial on the submesh) we obtain, with hidden constants as before,

$$\begin{aligned} |v_h - I_{\mathrm{av},h}^l v_h|_{H^1(\mathcal{T}_h;\mathbb{R})}^2 &\lesssim \sum_{T \in \mathcal{T}_h} h_T^{-2} \|v_h - I_{\mathrm{av},h}^l v_h\|_T^2 \\ &\lesssim \sum_{T \in \mathcal{T}_h} h_T^{-2} \sum_{F \in \mathcal{F}_{\mathcal{V},T}} h_F \|[v_h]_F\|_F^2 \\ &\lesssim \sum_{F \in \mathcal{F}_h} \sum_{T \in \mathcal{T}_{\mathcal{V},F}} h_F^{-1} \|[v_h]_F\|_F^2, \end{aligned}$$

where we have used (11) to pass to the second line while, to pass to the third line, we have invoked the mesh regularity to write $h_F h_T^{-2} \lesssim h_F^{-1}$ and we have exchanged the order of the sums after introducing the notation $\mathcal{T}_{\mathcal{V},F}$ for the set of mesh elements whose closure has nonzero intersection with the closure of F. Using again mesh regularity to infer that $\mathrm{card}(\mathcal{T}_{\mathcal{V},F})$ is bounded uniformly in h, we arrive at

$$|v_h - I_{\mathrm{av},h}^l v_h|_{H^1(\mathcal{T}_h;\mathbb{R})}^2 \lesssim \sum_{F \in \mathcal{F}_h} h_F^{-1} \|[v_h]_F\|_F^2. \tag{12}$$

We are now ready to prove the discrete Korn inequality.

Lemma 1 (Discrete Korn inequality)**.** *Let an integer $l \geq 1$ be fixed and set, for all $\boldsymbol{v}_h \in \mathbb{P}^l(\mathcal{T}_h;\mathbb{R}^d)$,*

$$\|\boldsymbol{v}_h\|_{\boldsymbol{\epsilon},h} \coloneqq \left(\|\boldsymbol{\nabla}_{\mathrm{s},h} \boldsymbol{v}_h\|^2 + |\boldsymbol{v}_h|_{\mathrm{j},h}^2 \right)^{\frac{1}{2}} \text{ and } |\boldsymbol{v}_h|_{\mathrm{j},h} \coloneqq \left(\sum_{F \in \mathcal{F}_h} h_F^{-1} \|[\boldsymbol{v}_h]_F\|_F^2 \right)^{\frac{1}{2}}, \tag{13}$$

where $\boldsymbol{\nabla}_{\mathrm{s},h} : H^1(\mathcal{T}_h;\mathbb{R}^d) \to L^2(\Omega;\mathbb{R}^{d\times d}_{\mathrm{sym}})$ is the broken symmetric gradient such that $(\boldsymbol{\nabla}_{\mathrm{s},h}\boldsymbol{v})_{|T} = \boldsymbol{\nabla}_{\mathrm{s}}\boldsymbol{v}_{|T}$ for any $T \in \mathcal{T}_h$. Then, for all $\boldsymbol{v}_h \in \mathbb{P}^l(\mathcal{T}_h;\mathbb{R}^d)$, it holds with hidden constant depending only on Ω, d, l, and the mesh regularity parameter:

$$|\boldsymbol{v}_h|_{H^1(\mathcal{T}_h;\mathbb{R}^d)} \lesssim \|\boldsymbol{v}_h\|_{\boldsymbol{\epsilon},h}. \tag{14}$$

Proof. The proof adapts the arguments of (Brenner, 2003, Lemma 2.2). We can write

$$\begin{aligned}|\boldsymbol{v}_h|^2_{H^1(\mathcal{T}_h;\mathbb{R}^d)} &\lesssim |\boldsymbol{I}^l_{\mathrm{av},h}\boldsymbol{v}_h|^2_{H^1(\Omega;\mathbb{R}^d)} + |\boldsymbol{v}_h - \boldsymbol{I}^l_{\mathrm{av},h}\boldsymbol{v}_h|^2_{H^1(\mathcal{T}_h;\mathbb{R}^d)}\\ &\lesssim \|\boldsymbol{\nabla}_{\mathrm{s}}\boldsymbol{I}^l_{\mathrm{av},h}\boldsymbol{v}_h\|^2 + |\boldsymbol{v}_h|^2_{\mathrm{j},h}\\ &\lesssim \|\boldsymbol{\nabla}_{\mathrm{s},h}\boldsymbol{v}_h\|^2 + \|\boldsymbol{\nabla}_{\mathrm{s},h}(\boldsymbol{I}^l_{\mathrm{av},h}\boldsymbol{v}_h - \boldsymbol{v}_h)\|^2 + |\boldsymbol{v}_h|^2_{\mathrm{j},h}\\ &\lesssim \|\boldsymbol{\nabla}_{\mathrm{s},h}\boldsymbol{v}_h\|^2 + |\boldsymbol{v}_h|^2_{\mathrm{j},h} = \|\boldsymbol{v}_h\|^2_{\boldsymbol{\epsilon},h},\end{aligned}$$

where we have inserted $\pm\boldsymbol{I}^l_{\mathrm{av},h}\boldsymbol{v}_h$ into the seminorm and used a triangle inequality in the first line, we have applied the first Korn inequality in $H^1_0(\Omega;\mathbb{R}^d)$ to the first term and invoked (12) for the second term after recalling the definition (13) of the jump seminorm in the second line, we have inserted $\pm\boldsymbol{\nabla}_{\mathrm{s},h}\boldsymbol{v}_h$ and used a triangle inequality to pass to the third line, we have invoked again (12) to estimate the second term in the right-hand side to pass to the fourth line, and we have used the definition (13) of the strain norm to conclude. □

Remark 2 (Korn–Poincaré inequality). Combining the discrete Poincaré inequality resulting from (Di Pietro and Ern, 2010, Theorem 6.1) (see also (Di Pietro and Ern, 2012, Theorem 5.3 and Corollary 5.4)) with (14), we infer that it holds, for all $\boldsymbol{v}_h \in \mathbb{P}^l(\mathcal{T}_h;\mathbb{R}^d)$,

$$\|\boldsymbol{v}_h\| \lesssim \|\boldsymbol{v}_h\|_{\boldsymbol{\epsilon},h}, \tag{15}$$

with hidden constant independent of h and $\boldsymbol{v}_h$.

4. Discretisation

4.1. Discrete space

Given a mesh $\mathcal{M}_h = (\mathcal{T}_h, \mathcal{F}_h)$, we define the following space of discrete unknowns:

$$\underline{\boldsymbol{U}}_h \coloneqq \left\{\underline{\boldsymbol{v}}_h = ((\boldsymbol{v}_T)_{T\in\mathcal{T}_h}, (\boldsymbol{v}_F)_{F\in\mathcal{F}_h}) \;:\; \boldsymbol{v}_T \in \mathbb{P}^0(T;\mathbb{R}^d) \quad \forall T\in\mathcal{T}_h \text{ and } \boldsymbol{v}_F \in \mathbb{P}^0(F;\mathbb{R}^d) \quad \forall F\in\mathcal{F}_h\right\}.$$

For all $\underline{\boldsymbol{v}}_h \in \underline{\boldsymbol{U}}_h$, we denote by $\boldsymbol{v}_h \in \mathbb{P}^0(\mathcal{T}_h;\mathbb{R}^d)$ the piecewise constant function obtained by patching element-based unknowns, that is,

$$(\boldsymbol{v}_h)_{|T} \coloneqq \boldsymbol{v}_T \qquad \forall T\in\mathcal{T}_h. \tag{16}$$

The restrictions of $\underline{\boldsymbol{U}}_h$ and $\underline{\boldsymbol{v}}_h \in \underline{\boldsymbol{U}}_h$ to a generic mesh element $T\in\mathcal{T}_h$ are respectively denoted by $\underline{\boldsymbol{U}}_T$ and $\underline{\boldsymbol{v}}_T = (\boldsymbol{v}_T, (\boldsymbol{v}_F)_{F\in\mathcal{F}_T})$. The vector of discrete variables corresponding to a smooth function on Ω is obtained via the global interpolation operator $\underline{\boldsymbol{I}}_h : H^1(\Omega;\mathbb{R}^d) \to \underline{\boldsymbol{U}}_h$ such that, for all $\boldsymbol{v}\in H^1(\Omega;\mathbb{R}^d)$,

$$\underline{\boldsymbol{I}}_h\boldsymbol{v} \coloneqq ((\boldsymbol{\pi}^0_T\boldsymbol{v}_{|T})_{T\in\mathcal{T}_h}, (\boldsymbol{\pi}^0_F\boldsymbol{v}_{|F})_{F\in\mathcal{F}_h}).$$

Its restriction to a generic mesh element $T\in\mathcal{T}_h$ is the local interpolator $\underline{\boldsymbol{I}}_T : H^1(T;\mathbb{R}^d) \to \underline{\boldsymbol{U}}_T$ such that, for all $\boldsymbol{v}\in H^1(T;\mathbb{R}^d)$,

$$\underline{\boldsymbol{I}}_T\boldsymbol{v} = (\boldsymbol{\pi}^0_T\boldsymbol{v}, (\boldsymbol{\pi}^0_F\boldsymbol{v}_{|F})_{F\in\mathcal{F}_T}). \tag{17}$$

The displacement is sought in the following subspace of $\underline{\boldsymbol{U}}_h$ that strongly incorporates the homogeneous Dirichlet boundary condition:

$$\underline{\boldsymbol{U}}_{h,0} \coloneqq \left\{\underline{\boldsymbol{v}}_h \in \underline{\boldsymbol{U}}_h \;:\; \boldsymbol{v}_F = \boldsymbol{0} \quad \forall F\in\mathcal{F}_h^{\mathrm{b}}\right\}.$$

4.2. Displacement reconstruction

Let a mesh element $T \in \mathcal{T}_h$ be fixed. We define the local displacement reconstruction operator $\boldsymbol{p}_T^1 : \underline{\boldsymbol{U}}_T \to \mathbb{P}^1(T;\mathbb{R}^d)$ such that, for all $\underline{\boldsymbol{v}}_T \in \underline{\boldsymbol{U}}_T$,

$$\boldsymbol{\nabla}\boldsymbol{p}_T^1\underline{\boldsymbol{v}}_T = \sum_{F\in\mathcal{F}_T}\frac{|F|}{|T|}(\boldsymbol{v}_F - \boldsymbol{v}_T)\otimes\boldsymbol{n}_{TF} \text{ and } \frac{1}{|T|}\int_T \boldsymbol{p}_T^1\underline{\boldsymbol{v}}_T = \boldsymbol{v}_T. \tag{18}$$

Remark 3 (Explicit expression for the displacement reconstruction operator). From (18), one can infer the following explicit expression for the displacement reconstruction operator: For all $\boldsymbol{x}\in T$,

$$\boldsymbol{p}_T^1(\boldsymbol{x}) = \boldsymbol{v}_T + \sum_{F\in\mathcal{F}_T}\frac{|F|}{|T|}(\boldsymbol{x}-\overline{\boldsymbol{x}}_T)\cdot\boldsymbol{n}_{TF}\,(\boldsymbol{v}_F - \boldsymbol{v}_T), \tag{19}$$

where $\overline{\boldsymbol{x}}_T \coloneqq \frac{1}{|T|}\int_T \boldsymbol{x}$ denotes the centroid of T.

Proposition 4 (Commutation properties for the displacement reconstruction)**.** *It holds, for all* $\boldsymbol{v}\in H^1(T;\mathbb{R}^d)$*,*

$$\boldsymbol{\nabla}(\boldsymbol{p}_T^1\underline{\boldsymbol{I}}_T\boldsymbol{v}) = \boldsymbol{\pi}_T^0(\boldsymbol{\nabla}\boldsymbol{v}) \text{ and } \boldsymbol{p}_T^1(\underline{\boldsymbol{I}}_T\boldsymbol{v}) = \boldsymbol{\varpi}_T^1\boldsymbol{v}. \tag{20}$$

Proof. Let $\boldsymbol{v}\in H^1(T;\mathbb{R}^d)$. Recalling the definition (17) of the local interpolator, we have that

$$\begin{aligned}
\boldsymbol{\nabla}\boldsymbol{p}_T^1\underline{\boldsymbol{I}}_T\boldsymbol{v} &= \sum_{F\in\mathcal{F}_T}\frac{|F|}{|T|}(\boldsymbol{\pi}_F^0\boldsymbol{v} - \boldsymbol{\pi}_T^0\boldsymbol{v})\otimes\boldsymbol{n}_{TF}\\
&= \frac{1}{|T|}\sum_{F\in\mathcal{F}_T}\int_F \boldsymbol{v}\otimes\boldsymbol{n}_{TF} - \frac{1}{|T|}\sum_{F\in\mathcal{F}_T}\int_F \boldsymbol{\pi}_T^0\boldsymbol{v}\otimes\boldsymbol{n}_{TF}\\
&= \frac{1}{|T|}\int_T \boldsymbol{\nabla}\boldsymbol{v} - \cancel{\frac{1}{|T|}\int_T \boldsymbol{\nabla}\boldsymbol{\pi}_T^0\boldsymbol{v}},
\end{aligned}$$

where we have used the definition (18) of the local displacement reconstruction with $\underline{\boldsymbol{v}}_T = \underline{\boldsymbol{I}}_T\boldsymbol{v}$ in the first line, the definition (5) of the L^2-orthogonal projector $\boldsymbol{\pi}_F^0$ along with the fact that $\boldsymbol{\pi}_T^0\boldsymbol{v}\otimes\boldsymbol{n}_{TF}$ is constant over F to pass to the second line, the Stokes theorem to pass to the third line and the fact that $\boldsymbol{\pi}_T^0\boldsymbol{v}$ is constant inside T to cancel the second term therein. This proves the first relation in (20). The second relation in (20) immediately follows accounting for the first and recalling the definition (8) of the elliptic projector after observing that the second relation in (18) gives

$$\frac{1}{|T|}\int_T \boldsymbol{p}_T^1\underline{\boldsymbol{I}}_T\boldsymbol{v} = \boldsymbol{\pi}_T^0\boldsymbol{v} = \frac{1}{|T|}\int_T \boldsymbol{v}.$$

□

To close this section, we define the global displacement reconstruction operator $\boldsymbol{p}_h^1 : \underline{\boldsymbol{U}}_h \to \mathbb{P}^1(\mathcal{T}_h;\mathbb{R}^d)$ obtained by patching the local reconstructions: For all $\underline{\boldsymbol{v}}_h\in\underline{\boldsymbol{U}}_h$,

$$(\boldsymbol{p}_h^1\underline{\boldsymbol{v}}_h)_{|T} \coloneqq \boldsymbol{p}_T^1\underline{\boldsymbol{v}}_T \qquad \forall T\in\mathcal{T}_h. \tag{21}$$

4.3. Discrete bilinear form

We define the bilinear form $\mathrm{a}_h : \underline{\boldsymbol{U}}_h\times\underline{\boldsymbol{U}}_h \to \mathbb{R}$ such that, for all $\underline{\boldsymbol{w}}_h,\underline{\boldsymbol{v}}_h\in\underline{\boldsymbol{U}}_h$,

$$\mathrm{a}_h(\underline{\boldsymbol{w}}_h,\underline{\boldsymbol{v}}_h) \coloneqq (\boldsymbol{\sigma}(\boldsymbol{\nabla}_{\mathrm{s},h}\boldsymbol{p}_h^1\underline{\boldsymbol{w}}_h), \boldsymbol{\nabla}_{\mathrm{s},h}\boldsymbol{p}_h^1\underline{\boldsymbol{v}}_h) + (2\mu)\,\mathrm{j}_h(\boldsymbol{p}_h^1\underline{\boldsymbol{w}}_h,\boldsymbol{p}_h^1\underline{\boldsymbol{v}}_h) + (2\mu)\,\mathrm{s}_h(\underline{\boldsymbol{w}}_h,\underline{\boldsymbol{v}}_h). \tag{22}$$

In the above expression, $\mathrm{j}_h : H^1(\mathcal{T}_h;\mathbb{R}^d)\times H^1(\mathcal{T}_h;\mathbb{R}^d)\to\mathbb{R}$ is the jump penalisation bilinear form such that, for all $\boldsymbol{w},\boldsymbol{v}\in H^1(\mathcal{T}_h;\mathbb{R}^d)$,

$$\mathrm{j}_h(\boldsymbol{w},\boldsymbol{v}) \coloneqq \sum_{F\in\mathcal{F}_h} h_F^{-1}([\boldsymbol{w}]_F,[\boldsymbol{v}]_F)_F,$$

while $\mathrm{s}_h : \underline{\boldsymbol{U}}_h \times \underline{\boldsymbol{U}}_h \to \mathbb{R}$ is a stabilisation bilinear form defined from local contributions as follows:

$$\mathrm{s}_h(\underline{\boldsymbol{w}}_h, \underline{\boldsymbol{v}}_h) \coloneqq \sum_{T\in\mathcal{T}_h} \mathrm{s}_T(\underline{\boldsymbol{w}}_T, \underline{\boldsymbol{v}}_T) \text{ with } \mathrm{s}_T(\underline{\boldsymbol{w}}_T, \underline{\boldsymbol{v}}_T) \coloneqq \sum_{F\in\mathcal{F}_T} \frac{|F|}{h_F} \boldsymbol{\delta}_{TF}\underline{\boldsymbol{w}}_T \cdot \boldsymbol{\delta}_{TF}\underline{\boldsymbol{v}}_T \text{ for all } T \in \mathcal{T}_h. \tag{23}$$

In the above expression, for all $T \in \mathcal{T}_h$ and all $F \in \mathcal{F}_T$, we have introduced the boundary difference operator $\boldsymbol{\delta}_{TF} : \underline{\boldsymbol{U}}_T \to \mathbb{R}^d$ is such that, for any $\underline{\boldsymbol{v}}_T \in \underline{\boldsymbol{U}}_T$,

$$\boldsymbol{\delta}_{TF}\underline{\boldsymbol{v}}_T \coloneqq \boldsymbol{\pi}^0_F \boldsymbol{p}^1_T \underline{\boldsymbol{v}}_T - \boldsymbol{v}_F. \tag{24}$$

It can be proved that the stabilisation bilinear form enjoys the following consistency property: For all $\boldsymbol{w} \in H^1(\Omega;\mathbb{R}^d) \cap H^2(\mathcal{T}_h;\mathbb{R}^d)$,

$$\mathrm{s}_h(\underline{\boldsymbol{I}}_h\boldsymbol{w}, \underline{\boldsymbol{I}}_h\boldsymbol{w})^{\frac12} \lesssim h|\boldsymbol{w}|_{H^2(\mathcal{T}_h;\mathbb{R}^d)}, \tag{25}$$

with hidden constant independent of both h and $\boldsymbol{w}$.

4.4. Comparison with the original HHO method and role of the jump penalisation term

Compared with the original HHO bilinear form defined by (Di Pietro and Ern, 2015, Eqs. (24)–(26) and (38)) and written for $k = 0$, the bilinear form (22) includes a novel jump penalisation contribution inspired by the discrete Korn inequality of Lemma 1. This term is needed for stability which, for HHO discretisations of the linear elasticity problem, cannot be achieved through local stabilisation terms for $k = 0$. As a matter of fact, following the ideas of (Di Pietro and Tittarelli, 2018, Section 4.3.1.4), stability would require the use in (23) of a family of local symmetric, positive semidefinite stabilisation bilinear forms $\{\mathrm{s}_T : T \in \mathcal{T}_h\}$ satisfying the following properties:

(i) *Local stability and boundedness.* For all $T \in \mathcal{T}_h$ and all $\underline{\boldsymbol{v}}_T \in \underline{\boldsymbol{U}}_T$, with hidden constants independent of h, T, and $\underline{\boldsymbol{v}}_T$,

$$\|\boldsymbol{\nabla}_{\mathrm{s}}\boldsymbol{p}^1_T\underline{\boldsymbol{v}}_T\|^2_T + \mathrm{s}_T(\underline{\boldsymbol{v}}_T, \underline{\boldsymbol{v}}_T) \simeq \sum_{F\in\mathcal{F}_T} h_F^{-1}\|\boldsymbol{v}_F - \boldsymbol{v}_T\|^2_F. \tag{26}$$

(ii) *Polynomial consistency.* For all $\boldsymbol{w} \in \mathbb{P}^{k+1}(T;\mathbb{R}^d)$,

$$\mathrm{s}_T(\underline{\boldsymbol{I}}_T\boldsymbol{w}, \underline{\boldsymbol{v}}_T) = 0 \qquad \forall \underline{\boldsymbol{v}}_T \in \underline{\boldsymbol{U}}_T. \tag{27}$$

Actually, as noticed in (Di Pietro and Droniou, 2019, Chapter 7), properties (26) and (27) are incompatible. To see it, assume (27), consider a rigid-body motion $\boldsymbol{v}_{\mathrm{rbm}}$, that is, a function over $\overline{T}$ for which there exist a vector $\boldsymbol{t}_{\boldsymbol{v}} \in \mathbb{R}^d$ and a skew-symmetric matrix $\boldsymbol{R}_{\boldsymbol{v}} \in \mathbb{R}^{d\times d}$ such that, for any $\boldsymbol{x} \in \overline{T}$, $\boldsymbol{v}_{\mathrm{rbm}}(\boldsymbol{x}) = \boldsymbol{t}_{\boldsymbol{v}} + \boldsymbol{R}_{\boldsymbol{v}}\boldsymbol{x}$. Take now $\underline{\boldsymbol{v}}_T = \underline{\boldsymbol{I}}_T\boldsymbol{v}_{\mathrm{rbm}}$. Since $\boldsymbol{v}_{\mathrm{rbm}} \in \mathbb{P}^1(T;\mathbb{R}^d)$, the first relation in (20) shows that $\boldsymbol{\nabla}\boldsymbol{p}^1_T\underline{\boldsymbol{v}}_T = \boldsymbol{\pi}^0_T(\boldsymbol{\nabla}\boldsymbol{v}_{\mathrm{rbm}}) = \boldsymbol{\nabla}\boldsymbol{v}_{\mathrm{rbm}} = \boldsymbol{R}_{\boldsymbol{v}}$ so that, in particular, $\boldsymbol{\nabla}\boldsymbol{p}^1_T\underline{\boldsymbol{v}}_T$ is skew-symmetric. Hence, $\boldsymbol{\nabla}_{\mathrm{s}}\boldsymbol{p}^1_T\underline{\boldsymbol{v}}_T = \boldsymbol{0}$. Moreover, by (27), $\mathrm{s}_T(\underline{\boldsymbol{v}}_T, \underline{\boldsymbol{v}}_T) = \mathrm{s}_T(\underline{\boldsymbol{I}}^0_T\boldsymbol{v}_{\mathrm{rbm}}, \underline{\boldsymbol{v}}_T) = 0$, again because $\boldsymbol{v}_{\mathrm{rbm}} \in \mathbb{P}^1(T;\mathbb{R}^d)$. Hence, the left-hand side of (26) vanishes for all $\underline{\boldsymbol{v}}_T = \underline{\boldsymbol{I}}_T\boldsymbol{v}_{\mathrm{rbm}}$ with $\boldsymbol{v}_{\mathrm{rbm}}$ rigid-body motion. It is, however, easy to construct a rigid-body motion $\boldsymbol{v}_{\mathrm{rbm}}$ such that the right-hand side does not vanish, which shows that (26) cannot hold. For this reason, the assumption that the discrete unknowns are at least piecewise affine is required in the original HHO method; see (Di Pietro and Ern, 2015, Section 4). Notice that the choice of s_T in (23) retains the polynomial consistency property (27), which is crucial to prove (25).

We next discuss how the stability property modifies for $k = 0$. To this end, recalling the definitions (13) of the double-bar strain norm $\|\cdot\|_{\boldsymbol{\varepsilon},h}$ and (23) of the stabilisation bilinear form we introduce the triple-bar strain norm such that, for any $\underline{\boldsymbol{v}}_h \in \underline{\boldsymbol{U}}_h$,

$$|||\underline{\boldsymbol{v}}_h|||_{\boldsymbol{\varepsilon},h} \coloneqq \left(\|\boldsymbol{p}^1_h\underline{\boldsymbol{v}}_h\|^2_{\boldsymbol{\varepsilon},h} + |\underline{\boldsymbol{v}}_h|^2_{\mathrm{s},h}\right)^{\frac12} \text{ with } |\underline{\boldsymbol{v}}_h|_{\mathrm{s},h} \coloneqq \mathrm{s}_h(\underline{\boldsymbol{v}}_h, \underline{\boldsymbol{v}}_h)^{\frac12}. \tag{28}$$

Lemma 5 (Global stability and boundedness)**.** *For all $\underline{\boldsymbol{v}}_h \in \underline{\boldsymbol{U}}_{h,0}$ it holds*

$$\|\boldsymbol{\nabla}_{\mathrm{s},h}\boldsymbol{p}^1_h\underline{\boldsymbol{v}}_h\|^2 + |\underline{\boldsymbol{v}}_h|^2_{\mathrm{s},h} \lesssim \sum_{T\in\mathcal{T}_h}\sum_{F\in\mathcal{F}_T} h_F^{-1}\|\boldsymbol{v}_F - \boldsymbol{v}_T\|^2_F \lesssim |||\underline{\boldsymbol{v}}_h|||^2_{\boldsymbol{\varepsilon},h}, \tag{29}$$

with hidden constant independent of both h and $\underline{\boldsymbol{v}}_h$.

Proof. It follows from (Di Pietro, Ern and Lemaire, 2014, Lemma 4) that

$$\|\boldsymbol{\nabla}_h \boldsymbol{p}_h^1 \underline{\boldsymbol{v}}_h\|^2 + |\underline{\boldsymbol{v}}_h|_{\mathrm{s},h}^2 \simeq \sum_{T\in\mathcal{T}_h}\sum_{F\in\mathcal{F}_T} h_F^{-1}\|\boldsymbol{v}_F - \boldsymbol{v}_T\|_F^2, \tag{30}$$

where $\boldsymbol{\nabla}_h : H^1(\mathcal{T}_h;\mathbb{R}^d) \to L^2(\Omega;\mathbb{R}^{d\times d})$ is the broken gradient such that $(\boldsymbol{\nabla}_h\boldsymbol{v})_{|T} = \boldsymbol{\nabla}\boldsymbol{v}_{|T}$ for any $T\in\mathcal{T}_h$. On the other hand, using the definition of the symmetric gradient for the first bound and Korn's inequality (14) for the second, we can write

$$\|\boldsymbol{\nabla}_{\mathrm{s},h} \boldsymbol{p}_h^1 \underline{\boldsymbol{v}}_h\|^2 \lesssim \|\boldsymbol{\nabla}_h \boldsymbol{p}_h^1 \underline{\boldsymbol{v}}_h\|^2 \lesssim \|\boldsymbol{\nabla}_{\mathrm{s},h} \boldsymbol{p}_h^1 \underline{\boldsymbol{v}}_h\|^2 + |\boldsymbol{p}_h^1 \boldsymbol{v}_h|_{\mathrm{j},h}^2. \tag{31}$$

Combining (31) with (30) yields the result. □

4.5. Discrete problem

The low-order scheme for the approximation of problem (1) reads: Find $\underline{\boldsymbol{u}}_h \in \underline{\boldsymbol{U}}_{h,0}$ such that

$$\mathrm{a}_h(\underline{\boldsymbol{u}}_h, \underline{\boldsymbol{v}}_h) = (\boldsymbol{f}, \boldsymbol{v}_h) \qquad \forall \underline{\boldsymbol{v}}_h \in \underline{\boldsymbol{U}}_{h,0}. \tag{32}$$

Using the coercivity of the bilinear form a_h proved in Lemma 8 below together with the discrete Korn inequality (15), we infer that the discrete problem is well-posed and the a priori estimate $|||\underline{\boldsymbol{u}}_h|||_{\boldsymbol{\epsilon},h} \lesssim \alpha^{-\frac{1}{2}}\|\boldsymbol{f}\|$ holds for the discrete solution, with hidden constant independent of both h and of the problem data, and triple-bar strain seminorm defined by (28).

Remark 6 (Static condensation for problem (32)). The jump stabilisation introduces a direct link among discrete unknowns attached to neighbouring mesh elements. As a result, static condensation of element-based unknowns no longer appears to be an interesting option.

Remark 7 (Nonlinear strain-stress laws). Following Botti et al. (2017), the method can be extended to nonlinear strain-stress laws $\boldsymbol{\sigma} : \mathbb{R}^{d\times d}_{\mathrm{sym}} \to \mathbb{R}^{d\times d}_{\mathrm{sym}}$ satisfying the regularity, growth, coercivity, and monotonicity assumptions detailed therein. We notice, in passing, that Lemma 1 along with (15) can be used to prove that assumption (Botti et al., 2017, Eq. (26)) holds on general meshes.

5. Convergence analysis

In this section, after studying the properties of the discrete bilinear form a_h, we prove a priori estimates for the error in the energy- and L^2-norms.

5.1. Properties of the discrete bilinear form

Lemma 8 (Properties of a_h)**.** *The bilinear form a_h enjoys the following properties:*

(i) Stability and boundedness. *Recalling the definition (28) of the triple-bar strain norm and the bound (3) on Lamé's coefficients, for all $\underline{\boldsymbol{v}}_h \in \underline{\boldsymbol{U}}_h$ it holds*

$$\alpha|||\underline{\boldsymbol{v}}_h|||_{\boldsymbol{\epsilon},h}^2 \lesssim \|\underline{\boldsymbol{v}}_h\|_{\mathrm{a},h}^2 \lesssim (2\mu + d|\lambda|)\,|||\underline{\boldsymbol{v}}_h|||_{\boldsymbol{\epsilon},h}^2 \text{ with } \|\underline{\boldsymbol{v}}_h\|_{\mathrm{a},h} \coloneqq \mathrm{a}_h(\underline{\boldsymbol{v}}_h, \underline{\boldsymbol{v}}_h)^{\frac{1}{2}}, \tag{33}$$

where the hidden constants are independent of both h and the problem data.

(ii) Consistency. *It holds for all $\boldsymbol{w} \in H_0^1(\Omega;\mathbb{R}^d) \cap H^2(\mathcal{T}_h;\mathbb{R}^d)$ such that $\boldsymbol{\nabla}\cdot\boldsymbol{\sigma}(\boldsymbol{\nabla}_{\mathrm{s}}\boldsymbol{w}) \in L^2(\Omega;\mathbb{R}^d)$,*

$$|||\mathcal{E}_h(\boldsymbol{w};\cdot)|||_{\boldsymbol{\epsilon},h,*} \lesssim h\left(2\mu|\boldsymbol{w}|_{H^2(\mathcal{T}_h;\mathbb{R}^d)} + |\lambda\boldsymbol{\nabla}\cdot\boldsymbol{w}|_{H^1(\mathcal{T}_h;\mathbb{R})}\right), \tag{34}$$

where the hidden constant is independent of $\boldsymbol{w}$, h, and of the problem data, the linear form $\mathcal{E}_h(\boldsymbol{w};\cdot) : \underline{\boldsymbol{U}}_{h,0} \to \mathbb{R}$ representing the consistency error is such that, for all $\underline{\boldsymbol{v}}_h \in \underline{\boldsymbol{U}}_{h,0}$,

$$\mathcal{E}_h(\boldsymbol{w};\underline{\boldsymbol{v}}_h) \coloneqq -(\boldsymbol{\nabla}\cdot\boldsymbol{\sigma}(\boldsymbol{\nabla}_{\mathrm{s}}\boldsymbol{w}), \boldsymbol{v}_h) - \mathrm{a}_h(\underline{\boldsymbol{I}}_h\boldsymbol{w}, \underline{\boldsymbol{v}}_h), \tag{35}$$

and its dual norm is given by

$$|||\mathcal{E}_h(\boldsymbol{w};\cdot)|||_{\boldsymbol{\epsilon},h,*} \coloneqq \sup_{\underline{\boldsymbol{v}}_h\in\underline{\boldsymbol{U}}_{h,0}, |||\underline{\boldsymbol{v}}_h|||_{\boldsymbol{\epsilon},h}=1} \left|\mathcal{E}_h(\boldsymbol{w};\underline{\boldsymbol{v}}_h)\right|.$$

Proof. (i) *Stability and boundedness.* Let $\underline{\boldsymbol{v}}_h \in \underline{\boldsymbol{U}}_h$. We recall the Frobenius product such that, for all $\boldsymbol{\tau}, \boldsymbol{\eta} \in \mathbb{R}^{d\times d}$, $\boldsymbol{\tau}:\boldsymbol{\eta} \coloneqq \sum_{i=1}^d \sum_{j=1}^d \tau_{ij}\eta_{ij}$ with corresponding norm $\|\boldsymbol{\tau}\|_{\mathrm{F}} \coloneqq (\boldsymbol{\tau}:\boldsymbol{\tau})^{\frac{1}{2}}$. Writing (22) for $\underline{\boldsymbol{w}}_h = \underline{\boldsymbol{v}}_h$, using the assumption (3) on Lamé's parameters to infer that $\boldsymbol{\sigma}(\boldsymbol{\tau}):\boldsymbol{\tau} \geq \alpha\|\boldsymbol{\tau}\|_{\mathrm{F}}^2$ for any $\boldsymbol{\tau} \in \mathbb{R}^{d\times d}_{\mathrm{sym}}$, recalling the definitions (13) and (28) of the double- and triple-bar strain norms, and observing that $2\mu \geq \alpha$, the first inequality in (33) follows. The second inequality can be obtained in a similar way: write (22) for $\underline{\boldsymbol{w}}_h = \underline{\boldsymbol{v}}_h$, observe that $|\boldsymbol{\sigma}(\boldsymbol{\tau}):\boldsymbol{\tau}| \leq (2\mu + d|\lambda|)\|\boldsymbol{\tau}\|_{\mathrm{F}}^2$ for any $\boldsymbol{\tau} \in \mathbb{R}^{d\times d}_{\mathrm{sym}}$, and use again (13) and (28).

(ii) *Consistency.* Let $\underline{\boldsymbol{v}}_h \in \underline{\boldsymbol{U}}_{h,0}$. We reformulate the components of the consistency error. Integrating by parts element by element, we infer that

$$-(\boldsymbol{\nabla}\cdot\boldsymbol{\sigma}(\boldsymbol{\nabla}_{\mathrm{s}}\boldsymbol{w}), \boldsymbol{v}_h) = \sum_{T\in\mathcal{T}_h}\sum_{F\in\mathcal{F}_T} (\boldsymbol{\sigma}(\boldsymbol{\nabla}_{\mathrm{s}}\boldsymbol{w})_{|T}\boldsymbol{n}_{TF}, \boldsymbol{v}_F - \boldsymbol{v}_T)_F,$$

where we have used the continuity of normal tractions across interfaces together with the fact that boundary unknowns are set to zero in $\underline{\boldsymbol{U}}_{h,0}$ to insert $\boldsymbol{v}_F$ into the right-hand side. To reformulate the second term in (35), in the expression (22) of a_h we use the first property in (20) together with the linearity of the strain-stress law $\boldsymbol{\sigma}$ to write, for all $T \in \mathcal{T}_h$, $\boldsymbol{\sigma}(\boldsymbol{\nabla}_{\mathrm{s}}p_T^1\underline{\boldsymbol{I}}_T\boldsymbol{w}) = \boldsymbol{\sigma}(\boldsymbol{\pi}_T^0(\boldsymbol{\nabla}_{\mathrm{s}}\boldsymbol{w})) = \boldsymbol{\pi}_T^0(\boldsymbol{\sigma}(\boldsymbol{\nabla}_{\mathrm{s}}\boldsymbol{w}))$ and obtain

$$\mathrm{a}_h(\underline{\boldsymbol{I}}_h\boldsymbol{w}, \underline{\boldsymbol{v}}_h) = \sum_{T\in\mathcal{T}_h} (\boldsymbol{\pi}_T^0(\boldsymbol{\sigma}(\boldsymbol{\nabla}_{\mathrm{s}}\boldsymbol{w})), \boldsymbol{\nabla}_{\mathrm{s}}p_T^1\underline{\boldsymbol{v}}_T)_T + (2\mu)\,\mathrm{j}_h(p_h^1\underline{\boldsymbol{I}}_h\boldsymbol{w}, p_h^1\underline{\boldsymbol{v}}_h) + (2\mu)\,\mathrm{s}_h(\underline{\boldsymbol{I}}_h\boldsymbol{w}, \underline{\boldsymbol{v}}_h).$$

After expanding, for all $T \in \mathcal{T}_h$, $\boldsymbol{\nabla}_{\mathrm{s}}p_T^1\underline{\boldsymbol{v}}_T$ according to its definition (18), we deduce that

$$\mathrm{a}_h(\underline{\boldsymbol{I}}_h\boldsymbol{w}, \underline{\boldsymbol{v}}_h) = \sum_{T\in\mathcal{T}_h}\sum_{F\in\mathcal{F}_T} (\boldsymbol{\pi}_T^0(\boldsymbol{\sigma}(\boldsymbol{\nabla}_{\mathrm{s}}\boldsymbol{w}))\boldsymbol{n}_{TF}, \boldsymbol{v}_F - \boldsymbol{v}_T)_F + (2\mu)\,\mathrm{j}_h(p_h^1\underline{\boldsymbol{I}}_h\boldsymbol{w}, p_h^1\underline{\boldsymbol{v}}_h) + (2\mu)\,\mathrm{s}_h(\underline{\boldsymbol{I}}_h\boldsymbol{w}, \underline{\boldsymbol{v}}_h).$$

Plugging the above relations into the expression (35) of the consistency error, passing to absolute values, using a generalised Hölder inequality with exponents $(2,\infty,2)$ along with $\|\boldsymbol{n}_{TF}\|_{L^\infty(F;\mathbb{R}^d)} \leq 1$ and $h_F \leq h_T$ for the first term in the right-hand side, and Cauchy–Schwarz inequalities for the remaining terms, we get

$$\begin{aligned}\left|\mathcal{E}_h(\boldsymbol{w};\underline{\boldsymbol{v}}_h)\right| &= \underbrace{\left(\sum_{T\in\mathcal{T}_h} h_T\|\boldsymbol{\sigma}(\boldsymbol{\nabla}_{\mathrm{s}}\boldsymbol{w})_{|T} - \boldsymbol{\pi}_T^0(\boldsymbol{\sigma}(\boldsymbol{\nabla}_{\mathrm{s}}\boldsymbol{w}))\|_{\partial T}^2\right)^{\frac{1}{2}}}_{\mathfrak{T}_1}\left(\sum_{T\in\mathcal{T}_h}\sum_{F\in\mathcal{F}_T} h_F^{-1}\|\boldsymbol{v}_F - \boldsymbol{v}_T\|_F^2\right)^{\frac{1}{2}}\\ &\quad + \underbrace{(2\mu)|p_h^1\underline{\boldsymbol{I}}_h\boldsymbol{w}|_{\mathrm{j},h}}_{\mathfrak{T}_2}\,|p_h^1\underline{\boldsymbol{v}}_h|_{\mathrm{j},h} + \underbrace{(2\mu)|\underline{\boldsymbol{I}}_h\boldsymbol{w}|_{\mathrm{s},h}}_{\mathfrak{T}_3}\,|\underline{\boldsymbol{v}}_h|_{\mathrm{s},h} \lesssim \left(\mathfrak{T}_1 + \mathfrak{T}_2 + \mathfrak{T}_3\right)|||\underline{\boldsymbol{v}}_h|||_{\epsilon,h},\end{aligned} \tag{36}$$

where we have used the second inequality in (29) together with the definition (28) of the triple-bar strain norm to conclude. Recalling the expression (2) of the strain-stress law, we get, for any $T \in \mathcal{T}_h$,

$$\begin{aligned}h_T^{\frac{1}{2}}\|\boldsymbol{\sigma}(\boldsymbol{\nabla}_{\mathrm{s}}\boldsymbol{w})_{|T} - \boldsymbol{\pi}_T^0(\boldsymbol{\sigma}(\boldsymbol{\nabla}_{\mathrm{s}}\boldsymbol{w}))\|_{\partial T} &\leq (2\mu)h_T^{\frac{1}{2}}\|\boldsymbol{\nabla}_{\mathrm{s}}\boldsymbol{w} - (\boldsymbol{\pi}_T^0\boldsymbol{\nabla}_{\mathrm{s}}\boldsymbol{w})\|_{\partial T} + h_T^{\frac{1}{2}}\|\lambda\boldsymbol{\nabla}\cdot\boldsymbol{w} - \pi_T^0(\lambda\boldsymbol{\nabla}\cdot\boldsymbol{w})\|_{\partial T}\\ &\lesssim h\left((2\mu)|\boldsymbol{w}|_{H^2(T;\mathbb{R}^d)} + |\lambda\boldsymbol{\nabla}\cdot\boldsymbol{w}|_{H^1(T;\mathbb{R})}\right),\end{aligned} \tag{37}$$

where we have used the approximation properties (6) of the L^2-orthogonal projector along with $h_T \leq h$ to conclude. Using the above estimate, we infer for the first term

$$\mathfrak{T}_1 \lesssim h\left((2\mu)|\boldsymbol{w}|_{H^2(\mathcal{T}_h;\mathbb{R}^d)} + |\lambda\boldsymbol{\nabla}\cdot\boldsymbol{w}|_{H^1(\mathcal{T}_h;\mathbb{R})}\right). \tag{38}$$

Moving to the second term, we start by observing that

$$\begin{aligned}
\mathfrak{T}_2^2 &= (2\mu)^2\, |\boldsymbol{\varpi}_h^1 \boldsymbol{w}|_{\mathrm{j},h}^2 \\
&= (2\mu)^2 \sum_{F\in\mathcal{F}_h} h_F^{-1} \|[\boldsymbol{\varpi}_h^1 \boldsymbol{w}]_F\|_F^2 \\
&= (2\mu)^2 \sum_{F\in\mathcal{F}_h} h_F^{-1} \|[\boldsymbol{\varpi}_h^1 \boldsymbol{w} - \boldsymbol{w}]_F\|_F^2 \\
&\lesssim (2\mu)^2 \sum_{F\in\mathcal{F}_h} \sum_{T\in\mathcal{T}_F} h_F^{-1} \|\boldsymbol{\varpi}_T^1 \boldsymbol{w} - \boldsymbol{w}_{|T}\|_F^2 \\
&\lesssim (2\mu)^2 \sum_{T\in\mathcal{T}_h} h_T^{-1} \|\boldsymbol{\varpi}_T^1 \boldsymbol{w} - \boldsymbol{w}_{|T}\|_{\partial T}^2
\end{aligned}$$

where we have used, in this order, the second relation in (20), the definition (13) of the jump seminorm, the fact that the jumps of $\boldsymbol{w}$ vanish across any $F \in \mathcal{F}_h$, the definition (10) of the jump operator together with the triangle inequality, and the relation

$$\sum_{T\in\mathcal{T}_h} \sum_{F\in\mathcal{F}_T} \bullet = \sum_{F\in\mathcal{F}_h} \sum_{T\in\mathcal{T}_F} \bullet \tag{39}$$

to exchange the sums over elements and faces. Hence, using the approximation properties (9) of the elliptic projector, $h_T \le h$, and taking the square root, we arrive at

$$\mathfrak{T}_2 \lesssim (2\mu) h |\boldsymbol{w}|_{H^2(\mathcal{T}_h;\mathbb{R}^d)}. \tag{40}$$

For the third term, (25) readily gives

$$\mathfrak{T}_3 \lesssim (2\mu) h |\boldsymbol{w}|_{H^2(\mathcal{T}_h;\mathbb{R}^d)}. \tag{41}$$

Plugging (38), (40), and (41) into (36) and passing to the supremum yields (34). □

5.2. Energy error estimate

Theorem 9 (Energy error estimate)**.** *Let $\boldsymbol{u} \in H_0^1(\Omega;\mathbb{R}^d)$ denote the unique solution to (4), for which we assume the additional regularity $\boldsymbol{u} \in H^2(\mathcal{T}_h;\mathbb{R}^d)$. For all $h \in \mathcal{H}$, let $\underline{\boldsymbol{u}}_h \in \underline{\boldsymbol{U}}_{h,0}$ denote the unique solution to (32). Then,*

$$|||\underline{\boldsymbol{u}}_h - \underline{\boldsymbol{I}}_h \boldsymbol{u}|||_{\epsilon,h} \lesssim \alpha^{-1} h \left((2\mu) |\boldsymbol{u}|_{H^2(\mathcal{T}_h;\mathbb{R}^d)} + |\lambda \boldsymbol{\nabla}\cdot\boldsymbol{u}|_{H^1(\mathcal{T}_h;\mathbb{R})} \right), \tag{42}$$

with hidden constant independent of h, $\boldsymbol{u}$, and of the problem data.

Proof. Applying to the present setting the results of (Di Pietro and Droniou, 2018, Theorem 10) gives the abstract estimate

$$|||\underline{\boldsymbol{u}}_h - \underline{\boldsymbol{I}}_h \boldsymbol{u}|||_{\epsilon,h} \le \alpha^{-1} |||\mathcal{E}_h(\boldsymbol{u};\cdot)|||_{\epsilon,h,*}.$$

Using the assumed regularity for the exact solution to invoke (34), (42) follows. □

Remark 10 (Robustness in the quasi-incompressible limit). In the numerical approximation of linear elasticity problems, a key point consists in devising schemes that are robust in the quasi incompressible limit corresponding to $\frac{\lambda}{2\mu} \gg 1$ (which requires, in particular $\lambda \ge 0$). From a mathematical perspective, this property is expressed by the fact that the error estimates are uniform in λ. For $d = 2$ and Ω convex, it is proved, e.g., in (Brenner and Sung, 1992, Lemma 2.2) that

$$(2\mu)\|\boldsymbol{u}\|_{H^2(\Omega;\mathbb{R}^d)} + \|\lambda \boldsymbol{\nabla}\cdot\boldsymbol{u}\|_{H^1(\Omega;\mathbb{R})} \lesssim \|\boldsymbol{f}\|, \tag{43}$$

with hidden constant possibly depending on Ω and μ but independent of λ. This result can be extended to $d = 3$ reasoning as in the above reference and accounting for the regularity estimates for the Stokes problem derived in

(Amrouche and Girault, 1991, Theorem 3). Plugging (43) into (42) and observing that, when $\lambda \geq 0$, we can take $\alpha = 2\mu$ (cf. (3)), we can write, with hidden constant independent of both h and λ,

$$|||\underline{\boldsymbol{u}}_h - \underline{\boldsymbol{I}}_h \boldsymbol{u}|||_{\epsilon,h} \lesssim h\|\boldsymbol{f}\|, \tag{44}$$

which shows that our error estimate (42) is uniform in λ. The key point to obtain robustness is the first commutation property in (20), which is used to estimate the term $\mathcal{T}_1$ in the proof of Lemma 8.

Remark 11 (Quasi-optimality of the error estimate). It follows from the second inequality in (33) that the bilinear form a_h is bounded with boundedness constant independent of h. Hence, following (Di Pietro and Droniou, 2018, Remark 11), the error estimate (42) is quasi-optimal.

Remark 12 (Energy estimate in the $\|\cdot\|_{\mathrm{a},h}$-norm for $\lambda \geq 0$). When $\lambda \geq 0$, a consistency estimate in h holds for $\|\mathcal{E}_h(\boldsymbol{w};\cdot)\|_{\mathrm{a},h,*}$, the norm of the consistency error linear form dual to $\|\cdot\|_{\mathrm{a},h}$ (see (33)). To see it, observe that, from (36) together with $(2\mu)^{\frac{1}{2}}|||\underline{\boldsymbol{v}}_h|||_{\epsilon,h} \leq \|\underline{\boldsymbol{v}}_h\|_{\mathrm{a},h}$ (a consequence of the assumption $\lambda \geq 0$), it follows $\left|\mathcal{E}_h(\boldsymbol{w};\underline{\boldsymbol{v}}_h)\right| \lesssim \left(\mathfrak{T}_1 + \mathfrak{T}_2 + \mathfrak{T}_3\right)(2\mu)^{-\frac{1}{2}}\|\underline{\boldsymbol{v}}_h\|_{\mathrm{a},h}$. Hence, passing to the supremum over $\left\{\underline{\boldsymbol{v}}_h \in \underline{\boldsymbol{U}}_{h,0} \ : \ \|\underline{\boldsymbol{v}}_h\|_{\mathrm{a},h} = 1\right\}$, we infer

$$\|\mathcal{E}_h(\boldsymbol{w};\cdot)\|_{\mathrm{a},h,*} \lesssim h\left((2\mu)^{\frac{1}{2}}|\boldsymbol{w}|_{H^2(\mathcal{T}_h;\mathbb{R}^d)} + (2\mu)^{-\frac{1}{2}}|\lambda\boldsymbol{\nabla}\cdot\boldsymbol{w}|_{H^1(\mathcal{T}_h;\mathbb{R})}\right).$$

Invoking again (Di Pietro and Droniou, 2018, Theorem 10), this time with $\underline{\boldsymbol{U}}_{h,0}$ equipped with the $\|\cdot\|_{\mathrm{a},h}$-norm, it is inferred

$$\|\underline{\boldsymbol{u}}_h - \underline{\boldsymbol{I}}_h\boldsymbol{u}\|_{\mathrm{a},h} \lesssim h\left((2\mu)^{\frac{1}{2}}|\boldsymbol{u}|_{H^2(\mathcal{T}_h;\mathbb{R}^d)} + (2\mu)^{-\frac{1}{2}}|\lambda\boldsymbol{\nabla}\cdot\boldsymbol{u}|_{H^1(\mathcal{T}_h;\mathbb{R})}\right),$$

with hidden constant having the same dependencies as in (42).

5.3. Improved L^2-error estimate

It is well-known that improved L^2-error estimates can be derived in the context of HHO methods when elliptic regularity holds. In this section, we show that the same is true for the low-order method considered in this work. For the sake of simplicity, we assume throughout this section that

$$\lambda \geq 0.$$

This assumption could be removed, but we keep it here to simplify the discussion and point out the robustness in the quasi-incompressible limit. Recalling the discussion in Remark 10, elliptic regularity for our problem entails that, for all $\boldsymbol{g} \in L^2(\Omega;\mathbb{R}^d)$, the unique solution of the (dual) problem: Find $\boldsymbol{z}_{\boldsymbol{g}} \in H^1_0(\Omega;\mathbb{R}^d)$ such that

$$(\boldsymbol{\sigma}(\boldsymbol{\nabla}_{\mathrm{s}}\boldsymbol{z}_{\boldsymbol{g}}), \boldsymbol{\nabla}_{\mathrm{s}}\boldsymbol{v}) = (\boldsymbol{g},\boldsymbol{v}) \qquad \forall \boldsymbol{v} \in H^1_0(\Omega;\mathbb{R}^d) \tag{45}$$

satisfies the a priori estimate

$$(2\mu)\,\|\boldsymbol{z}_{\boldsymbol{g}}\|_{H^2(\Omega;\mathbb{R}^d)} + \|\lambda\boldsymbol{\nabla}\cdot\boldsymbol{z}_{\boldsymbol{g}}\|_{H^1(\Omega;\mathbb{R})} \lesssim \|\boldsymbol{g}\|, \tag{46}$$

with hidden constant only depending on Ω and μ.

Theorem 13 (Improved L^2-error estimate)**.** *Under the assumptions and notations of Theorem 9, and further assuming $\lambda \geq 0$, elliptic regularity, and $\boldsymbol{f} \in H^1(\mathcal{T}_h;\mathbb{R}^d)$, it holds that*

$$\|\boldsymbol{u}_h - \boldsymbol{\pi}^0_h\boldsymbol{u}\| \lesssim h^2\|\boldsymbol{f}\|_{H^1(\mathcal{T}_h;\mathbb{R}^d)}, \tag{47}$$

where the hidden constant is independent of both h and λ (but possibly depends on μ).

Proof. Inside the proof, hidden constants have the same dependencies as in (47). Applying the results of (Di Pietro and Droniou, 2018, Theorem 13) to the present setting gives the basic estimate

$$\|\boldsymbol{u}_h - \boldsymbol{\pi}^0_h\boldsymbol{u}\| \leq |||\underline{\boldsymbol{u}}_h - \underline{\boldsymbol{I}}_h\boldsymbol{u}|||_{\epsilon,h} \sup_{\boldsymbol{g}\in L^2(\Omega;\mathbb{R}^d),\|\boldsymbol{g}\|\leq 1} |||\mathcal{E}_h(\boldsymbol{z}_{\boldsymbol{g}};\cdot)|||_{\epsilon,h,*} + \sup_{\boldsymbol{g}\in L^2(\Omega;\mathbb{R}^d),\|\boldsymbol{g}\|\leq 1} \mathcal{E}_h(\boldsymbol{u};\underline{\boldsymbol{I}}_h\boldsymbol{z}_{\boldsymbol{g}}). \tag{48}$$

We proceed to bound the addends in the right-hand side, denoted for the sake of brevity $\mathfrak{T}_1$ and $\mathfrak{T}_2$.

(i) *Estimate of* $\mathfrak{T}_1$. Since $\boldsymbol{z}_{\boldsymbol{g}} \in H^1_0(\Omega;\mathbb{R}^d)\cap H^2(\Omega;\mathbb{R}^d)$, the consistency estimate (34) followed by the elliptic regularity bound (46) yield, for any $\boldsymbol{g} \in L^2(\Omega;\mathbb{R}^d)$,

$$|||\mathcal{E}_h(\boldsymbol{z}_{\boldsymbol{g}};\cdot)|||_{\boldsymbol{\epsilon},h,*} \lesssim h\left((2\mu)|\boldsymbol{z}_{\boldsymbol{g}}|_{H^2(\mathcal{T}_h;\mathbb{R}^d)} + |\lambda\boldsymbol{\nabla}\cdot\boldsymbol{z}_{\boldsymbol{g}}|_{H^1(\mathcal{T}_h;\mathbb{R})}\right) \lesssim h\|\boldsymbol{g}\|.$$

Combined with the energy error estimate (44), this yields

$$\mathfrak{T}_1 \lesssim h^2\|\boldsymbol{f}\|. \tag{49}$$

(ii) *Estimate of* $\mathfrak{T}_2$. Recalling the expression (35) of the consistency error, expanding the bilinear form a_h according to its definition (22) with $\underline{\boldsymbol{w}}_h = \underline{\boldsymbol{I}}_h\boldsymbol{u}$ and $\underline{\boldsymbol{v}}_h = \underline{\boldsymbol{I}}_h\boldsymbol{z}_{\boldsymbol{g}}$, and invoking (20) to replace $\boldsymbol{p}^1_h\underline{\boldsymbol{I}}_h$ with $\boldsymbol{\varpi}^1_h$ and $\boldsymbol{\nabla}_{\mathrm{s},h}\boldsymbol{p}^1_h\underline{\boldsymbol{I}}_h$ with $\boldsymbol{\pi}^0_h\boldsymbol{\nabla}_{\mathrm{s}}$, we can write

$$\mathcal{E}_h(\boldsymbol{u};\underline{\boldsymbol{I}}_h\boldsymbol{z}_{\boldsymbol{g}}) = (-\boldsymbol{\nabla}\cdot\boldsymbol{\sigma}(\boldsymbol{\nabla}_{\mathrm{s}}\boldsymbol{u}),\boldsymbol{\pi}^0_h\boldsymbol{z}_{\boldsymbol{g}}) - (\boldsymbol{\pi}^0_h(\boldsymbol{\sigma}(\boldsymbol{\nabla}_{\mathrm{s}}\boldsymbol{u})),\boldsymbol{\pi}^0_h\boldsymbol{\nabla}_{\mathrm{s}}\boldsymbol{z}_{\boldsymbol{g}}) - (2\mu)\,\mathrm{j}_h(\boldsymbol{\varpi}^1_h\boldsymbol{u},\boldsymbol{\varpi}^1_h\boldsymbol{z}_{\boldsymbol{g}}) - (2\mu)\,\mathrm{s}_h(\underline{\boldsymbol{I}}_h\boldsymbol{u},\underline{\boldsymbol{I}}_h\boldsymbol{z}_{\boldsymbol{g}}). \tag{50}$$

We have that

$$\begin{aligned}
-(\boldsymbol{\nabla}\cdot\boldsymbol{\sigma}(\boldsymbol{\nabla}_{\mathrm{s}}\boldsymbol{u}),\boldsymbol{\pi}^0_h\boldsymbol{z}_{\boldsymbol{g}}) = (\boldsymbol{f},\boldsymbol{\pi}^0_h\boldsymbol{z}_{\boldsymbol{g}}) &= (\boldsymbol{\pi}^0_h\boldsymbol{f},\boldsymbol{z}_{\boldsymbol{g}})\\
&= (\boldsymbol{\pi}^0_h\boldsymbol{f}-\boldsymbol{f},\boldsymbol{z}_{\boldsymbol{g}}) + (\boldsymbol{\sigma}(\boldsymbol{\nabla}_{\mathrm{s}}\boldsymbol{u}),\boldsymbol{\nabla}_{\mathrm{s}}\boldsymbol{z}_{\boldsymbol{g}})\\
&= (\boldsymbol{\pi}^0_h\boldsymbol{f}-\boldsymbol{f},\boldsymbol{z}_{\boldsymbol{g}}-\boldsymbol{\pi}^0_h\boldsymbol{z}_{\boldsymbol{g}}) + (\boldsymbol{\sigma}(\boldsymbol{\nabla}_{\mathrm{s}}\boldsymbol{u}),\boldsymbol{\nabla}_{\mathrm{s}}\boldsymbol{z}_{\boldsymbol{g}}),
\end{aligned}$$

where we have used the fact that (1a) holds almost everywhere in Ω to replace $-\boldsymbol{\nabla}\cdot\boldsymbol{\sigma}(\boldsymbol{\nabla}_{\mathrm{s}}\boldsymbol{u})$ with $\boldsymbol{f}$ along with the definitions (7) and (5) of the global and local L^2-orthogonal projectors in the first line, we have added the quantity $(\boldsymbol{f},\boldsymbol{z}_{\boldsymbol{g}}) - (\boldsymbol{\sigma}(\boldsymbol{\nabla}_{\mathrm{s}}\boldsymbol{u}),\boldsymbol{\nabla}_{\mathrm{s}}\boldsymbol{z}_{\boldsymbol{g}}) = 0$ (see (4)) in the second line, while, to pass to the third line, we have used the fact that, by definition of $\boldsymbol{\pi}^0_h$, the function $(\boldsymbol{\pi}^0_h\boldsymbol{f}-\boldsymbol{f})$ is $L^2(\Omega;\mathbb{R}^d)$-orthogonal to $\mathbb{P}^0(\mathcal{T}_h;\mathbb{R}^d)$ to insert $\boldsymbol{\pi}^0_h\boldsymbol{z}_{\boldsymbol{g}}$ into the first term. The Cauchy–Schwarz inequality and the approximation property (6) of the L^2-orthogonal projector inside each mesh element yield for the first term in the right-hand side

$$\left|(\boldsymbol{\pi}^0_h\boldsymbol{f}-\boldsymbol{f},\boldsymbol{z}_{\boldsymbol{g}}-\boldsymbol{\pi}^0_h\boldsymbol{z}_{\boldsymbol{g}})\right| \lesssim h^2|\boldsymbol{f}|_{H^1(\mathcal{T}_h;\mathbb{R}^d)}|\boldsymbol{z}_{\boldsymbol{g}}|_{H^1(\Omega;\mathbb{R}^d)} \lesssim h^2|\boldsymbol{f}|_{H^1(\mathcal{T}_h;\mathbb{R}^d)}\|\boldsymbol{g}\|, \tag{51}$$

where we have used a standard estimate on $|\boldsymbol{z}_{\boldsymbol{g}}|_{H^1(\Omega;\mathbb{R}^d)}$ obtained letting $\boldsymbol{v} = \boldsymbol{z}_{\boldsymbol{g}}$ in (45) and using the Cauchy–Schwarz and Korn inequalities to bound the right-hand side. On the other hand, using the definitions (7) and (5) of the global and local L^2-orthogonal projectors, we can write

$$\begin{aligned}
\left|\left(\boldsymbol{\sigma}(\boldsymbol{\nabla}_{\mathrm{s}}\boldsymbol{u}),\boldsymbol{\nabla}_{\mathrm{s}}\boldsymbol{z}_{\boldsymbol{g}}\right) - \left(\boldsymbol{\pi}^0_h(\boldsymbol{\sigma}(\boldsymbol{\nabla}_{\mathrm{s}}\boldsymbol{u})),\boldsymbol{\pi}^0_h\boldsymbol{\nabla}_{\mathrm{s}}\boldsymbol{z}_{\boldsymbol{g}}\right)\right| &= \left|\left(\boldsymbol{\sigma}(\boldsymbol{\nabla}_{\mathrm{s}}\boldsymbol{u}) - \boldsymbol{\pi}^0_h(\boldsymbol{\sigma}(\boldsymbol{\nabla}_{\mathrm{s}}\boldsymbol{u})),\boldsymbol{\nabla}_{\mathrm{s}}\boldsymbol{z}_{\boldsymbol{g}} - \boldsymbol{\pi}^0_h(\boldsymbol{\nabla}_{\mathrm{s}}\boldsymbol{z}_{\boldsymbol{g}})\right)\right|\\
&\le \|\boldsymbol{\sigma}(\boldsymbol{\nabla}_{\mathrm{s}}\boldsymbol{u}) - \boldsymbol{\pi}^0_h(\boldsymbol{\sigma}(\boldsymbol{\nabla}_{\mathrm{s}}\boldsymbol{u}))\|\ \|\boldsymbol{\nabla}_{\mathrm{s}}\boldsymbol{z}_{\boldsymbol{g}} - \boldsymbol{\pi}^0_h(\boldsymbol{\nabla}_{\mathrm{s}}\boldsymbol{z}_{\boldsymbol{g}})\|\\
&\lesssim h^2\left((2\mu)|\boldsymbol{u}|_{H^2(\Omega;\mathbb{R}^d)} + |\lambda\boldsymbol{\nabla}\cdot\boldsymbol{u}|_{H^1(\Omega;\mathbb{R}^d)}\right)|\boldsymbol{z}_{\boldsymbol{g}}|_{H^2(\Omega;\mathbb{R}^d)}\\
&\lesssim h^2\|\boldsymbol{f}\|\ \|\boldsymbol{g}\|,
\end{aligned} \tag{52}$$

where we have used a Cauchy–Schwarz inequality to pass to the third line, (37) with $\boldsymbol{w} = \boldsymbol{u}$ together with the approximation property (6) of the L^2-orthogonal projector to pass to the fourth line, and the elliptic regularity bound (46) to conclude. Finally, using Cauchy–Schwarz inequalities, we can write

$$\begin{aligned}
(2\mu)\,\mathrm{j}_h(\boldsymbol{\varpi}^1_h\boldsymbol{u},\boldsymbol{\varpi}^1_h\boldsymbol{z}_{\boldsymbol{g}}) + (2\mu)\,\mathrm{s}_h(\underline{\boldsymbol{I}}_h\boldsymbol{u},\underline{\boldsymbol{I}}_h\boldsymbol{z}_{\boldsymbol{g}}) &\lesssim (2\mu)\,|\boldsymbol{\varpi}^1_h\boldsymbol{u}|_{\mathrm{j},h}|\boldsymbol{\varpi}^1_h\boldsymbol{z}_{\boldsymbol{g}}|_{\mathrm{j},h} + (2\mu)\,|\underline{\boldsymbol{I}}_h\boldsymbol{u}|_{\mathrm{s},h}|\underline{\boldsymbol{I}}_h\boldsymbol{z}_{\boldsymbol{g}}|_{\mathrm{s},h}\\
&\lesssim (2\mu)h^2|\boldsymbol{u}|_{H^2(\Omega;\mathbb{R}^d)}|\boldsymbol{z}_{\boldsymbol{g}}|_{H^2(\Omega;\mathbb{R}^d)} \lesssim h^2\|\boldsymbol{f}\|\ \|\boldsymbol{g}\|,
\end{aligned} \tag{53}$$

where, to pass to the second line, we have used (25) for the terms involving s_h and we have proceeded as in the estimate of $\mathfrak{T}_2$ in the proof of point (ii) of Lemma 8 for the terms involving j_h while, to conclude, we have invoked (46). Taking absolute values in (50) and using the estimates (51), (52), (53) yields $\left|\mathcal{E}_h(\boldsymbol{u};\underline{\boldsymbol{I}}_h\boldsymbol{z}_{\boldsymbol{g}})\right| \lesssim h^2\|\boldsymbol{f}\|_{H^1(\mathcal{T}_h;\mathbb{R}^d)}\|\boldsymbol{g}\|$. Hence, passing to the supremum, we obtain

$$\mathfrak{T}_2 \lesssim h^2\|\boldsymbol{f}\|_{H^1(\mathcal{T}_h;\mathbb{R}^d)}. \tag{54}$$

Plugging (49) and (54) into (48) concludes the proof. □

Corollary 14 (L^2-error estimate for the displacement reconstruction)**.** *Under the notations and assumptions of Theorem 13, it holds*

$$\|\boldsymbol{p}_h^1\underline{\boldsymbol{u}}_h - \boldsymbol{u}\| \lesssim h^2\|\boldsymbol{f}\|_{H^1(\mathcal{T}_h;\mathbb{R}^d)}, \tag{55}$$

Proof. Inserting $\mathbf{0} = \boldsymbol{p}_h^1\underline{\boldsymbol{I}}_h\boldsymbol{u} - \boldsymbol{\varpi}_h^1\boldsymbol{u}$ inside the norm in the left-hand side of (55) and using the triangle inequality, we infer that

$$\|\boldsymbol{p}_h^1\underline{\boldsymbol{u}}_h - \boldsymbol{u}\| \le \|\boldsymbol{u} - \boldsymbol{\varpi}_h^1\boldsymbol{u}\| + \|\boldsymbol{p}_h^1(\underline{\boldsymbol{I}}_h\boldsymbol{u} - \underline{\boldsymbol{u}}_h)\| =: \mathfrak{T}_1 + \mathfrak{T}_2.$$

Combining the approximation properties (9) of the elliptic projector with elliptic regularity estimate (46) readily gives for the first term

$$\mathfrak{T}_1 \lesssim h^2\|\boldsymbol{f}\|.$$

For the second term, on the other hand, we observe that

$$\begin{aligned}
\mathfrak{T}_2^2 &= \sum_{T\in\mathcal{T}_h} \|\boldsymbol{p}_T^1(\underline{\boldsymbol{I}}_T\boldsymbol{u} - \underline{\boldsymbol{u}}_T)\|_T^2\\
&\lesssim \sum_{T\in\mathcal{T}_h} \left(h_T^2\|\boldsymbol{\nabla}\boldsymbol{p}_T^1(\underline{\boldsymbol{I}}_T\boldsymbol{u} - \underline{\boldsymbol{u}}_T)\|_T^2 + \|\boldsymbol{\pi}_T^0\boldsymbol{u} - \boldsymbol{u}_T\|_T^2\right)\\
&\le h^2\|\boldsymbol{\nabla}_h\boldsymbol{p}_h^1(\underline{\boldsymbol{I}}_h\boldsymbol{u} - \underline{\boldsymbol{u}}_h)\|^2 + \|\boldsymbol{\pi}_h^0\boldsymbol{u} - \boldsymbol{u}_h\|^2\\
&\lesssim h^2|||\underline{\boldsymbol{I}}_h\boldsymbol{u} - \underline{\boldsymbol{u}}_h|||_{\varepsilon,h}^2 + \|\boldsymbol{\pi}_T^0\boldsymbol{u} - \boldsymbol{u}_h\|^2 \lesssim h^2\|\boldsymbol{f}\|_{H^1(\mathcal{T}_h;\mathbb{R}^d)}^2,
\end{aligned}$$

where the second line follows from a local Poincaré–Wirtinger inequality together with the boundedness of the L^2-orthogonal projector, the fourth line is a consequence of the global Korn inequality (14) together with the definition (28) of the triple-bar strain norm, while the conclusion follows from the estimates (44) and (47). □

6. Numerical tests

In what follows we verify, through numerical examples, the results stated in the previous section. In order to assess the performance of the method in a framework as close as possible to real-life situations, we focus on the element shapes most frequently used in the engineering community.

6.1. Two-dimensional quasi-incompressible case

The first test case is inspired by Brenner (1993): we solve on the unit square $\Omega = (0,1)^2$ the homogeneous Dirichlet problem corresponding to the exact solution such that

$$\boldsymbol{u}(\boldsymbol{x}) = \begin{pmatrix} (\cos(2\pi x_1) - 1)\sin(2\pi x_2) + \frac{1}{1+\lambda}\sin(\pi x_1)\sin(\pi x_2)\\ (1 - \cos(2\pi x_2))\sin(2\pi x_1) + \frac{1}{1+\lambda}\sin(\pi x_1)\sin(\pi x_2)\end{pmatrix}.$$

The corresponding forcing term is

$$\boldsymbol{f}(\boldsymbol{x}) = \begin{pmatrix} -\mu\left[4\sin(2\pi x_2)\left(1 - 2\cos(2\pi x_1)\right) - \frac{2}{1+\lambda}\sin(\pi x_1)\sin(\pi x_2)\right] - \frac{\lambda+\mu}{1+\lambda}\cos(\pi(x_1+x_2))\\ -\mu\left[4\sin(2\pi x_1)\left(2\cos(2\pi x_2) - 1\right) - \frac{2}{1+\lambda}\sin(\pi x_1)\sin(\pi x_2)\right] - \frac{\lambda+\mu}{1+\lambda}\cos(\pi(x_1+x_2))\end{pmatrix}.$$

We take $\mu = 1$ and, in order to assess the robustness of the method in the quasi-incompressible limit, we let λ vary in $\{1, 10^3, 10^6\}$. For the numerical solution, we consider structured and unstructured triangular, Cartesian orthogonal, and deformed quadrangular mesh families; see Figure 1. The solutions corresponding to $\lambda = 1$ and $\lambda = 10^6$ on the finest Cartesian orthogonal mesh are represented in Figure 2, where we have plotted the components of the global displacement reconstruction obtained from the discrete solution according to (21).

The numerical results are collected in Tables 1–4, where the following quantities are monitored: $N_{\mathrm{dofs},h}$, the number of degrees of freedom; $N_{\mathrm{nz},h}$, the number of non-zero entries in the problem matrix; $|||\underline{\boldsymbol{u}}_h - \underline{\boldsymbol{I}}_h\boldsymbol{u}|||_{\mathrm{a},h}$, the

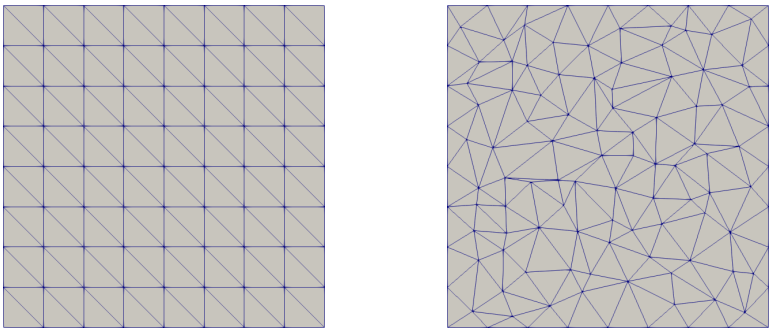

(a) Structured triangular mesh

(b) Unstructured triangular mesh

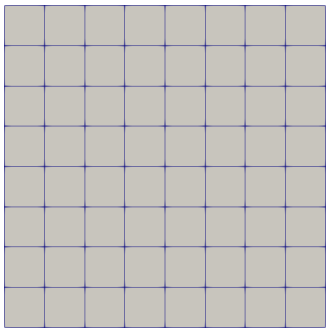

(c) Cartesian orthogonal mesh

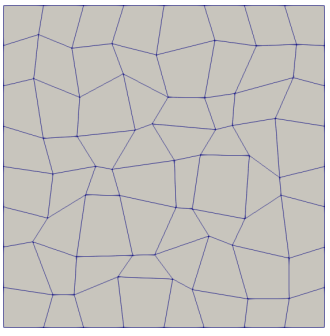

(d) Distorted quadrangular mesh

Figure 1: Meshes for the numerical test of Section 6.1.

energy-norm of the error; $\|\boldsymbol{u}_h - \boldsymbol{\pi}_h^0 \boldsymbol{u}\|$, the L^2-norm of the error estimated in Theorem 13. Notice that, in view of Remark 12, in this and in the following numerical tests the energy error is measured using the $\|\cdot\|_{\mathrm{a},h}$-norm, whose computation can be done using the already assembled problem matrix. We additionally display the Estimated Order of Convergence (EOC) which, denoting by e_i an error measure on the ith mesh refinement with meshsize h_i, is computed as

$$\mathrm{EOC} = \frac{\log e_i - \log e_{i+1}}{\log h_i - \log h_{i+1}}.$$

In all the cases, the asymptotic EOC match the ones predicted by the theory, that is, 1 for the energy-norm of the error and 2 for the L^2-norm. The results additionally highlight the robustness of the method in the quasi-incompressible limit (see Remark 10) and with respect to the mesh, showing errors of comparable magnitude irrespectively of the value of λ and of the selected mesh family.

6.2. Two-dimensional singular case

We next consider the solution of (Ainsworth and Senior, 1997, Section 5.1) which, in polar coordinates (r, θ), reads

$$\boldsymbol{u}(r,\theta) = \begin{pmatrix} \frac{1}{2G} r^L \left[(\kappa - Q(L+1))\cos(L\theta) - L\cos((L-2)\theta)\right] \\ \frac{1}{2G} r^L \left[(\kappa + Q(L+1))\sin(L\theta) + L\sin((L-2)\theta)\right] \end{pmatrix},$$

where the various parameters take the following numerical values: $\mu = 0.65$, $\lambda = 0.98$, $G = \frac{5}{13}$, $\kappa = \frac{9}{5}$, $L = 0.5444837367825$, $Q = 0.5430755788367$. The forcing term in this case is equal to zero, while the Dirichlet boundary condition is inferred from the exact solution. The domain Ω is illustrated in Figure 3, while the solution on the finest computational mesh considered here is depicted in Figure 4. This test case is representative of real-life situations corresponding to a mode 1 fracture in a plain strain problem. The solution exhibits a singularity in the origin, which prevents the method from attaining the full orders of convergence predicted for smooth solutions.

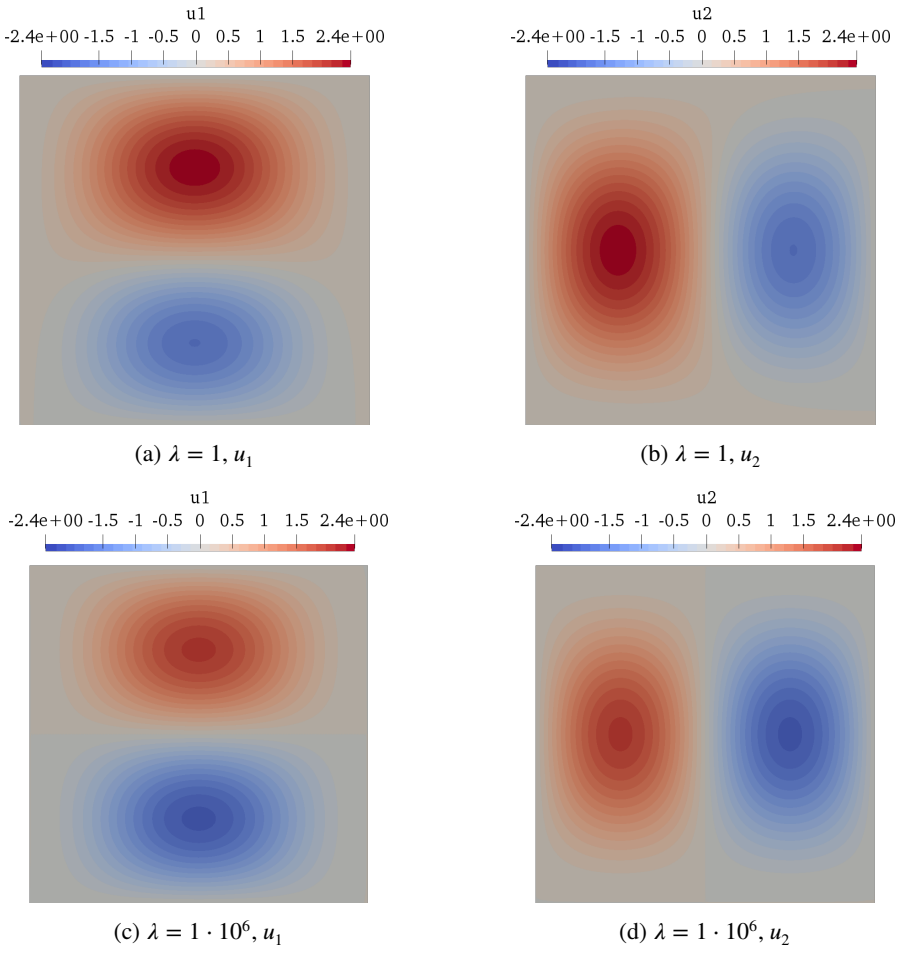

(a) $\lambda = 1, u_1$ (b) $\lambda = 1, u_2$

(c) $\lambda = 1 \cdot 10^6, u_1$ (d) $\lambda = 1 \cdot 10^6, u_2$

Figure 2: Numerical solution for the test of Section 6.1 on the 128×128 Cartesian orthogonal mesh.

For the numerical resolution, we consider a sequence of refined structured quadrangular meshes. The numerical results collected in the top half of Table 5 show an asymptotic EOC in the energy-norm of about 0.54, while the asymptotic EOC in the L^2-norm is about 1.31. For the sake of completeness, we show, in the bottom half of Table 5, a comparison with the original HHO method of Di Pietro and Ern (2015) with $k = 1$. Also in this case, the EOC are limited by the regularity of the solution, and coincide with those observed for the method studied in this work. As expected, the number of unknowns on a given mesh is larger for the method of Di Pietro and Ern (2015) compared to the method proposed here, despite the fact that static condensation is applied in the former case. It has to be noticed, however, that the reduction in the number of unknowns is balanced by the increased number of nonzero entries in the matrix, due to both the absence of static condensation (see Remark 6) and the presence of the jump penalisation term. This phenomenon is specific to the two-dimensional case: in dimension $d = 3$, the matrix corresponding to the method of Di Pietro and Ern (2015) with $k = 1$ is generally more dense; see, e.g., Table 6. The errors in the energy norm appear to be smaller for the HHO method of Di Pietro and Ern (2015), but this is in part due to the fact that the natural energy norm associated with the corresponding bilinear form does not contain the norm of the jumps.

6.3. Three-dimensional compressible case

To test the performance of the method in three space dimensions, we solve on the unit cube domain $\Omega = (0,1)^3$ the homogeneous Dirichlet problem corresponding to the exact solution $\boldsymbol{u} = (u_i)_{1\le i\le d}$ such that

$$u_i(\boldsymbol{x}) = \sin(\pi x_1)\sin(\pi x_2)\sin(\pi x_3) \qquad \forall 1 \le i \le 3.$$

Table 1
Numerical results for the test of Section 6.1, structured triangular mesh family.

$N_{\mathrm{dofs},h}$	$N_{\mathrm{nz},h}$	$\|\underline{\boldsymbol{u}}_h - \underline{\boldsymbol{I}}_h \boldsymbol{u}\|_{\mathrm{a},h}$	EOC	$\|\boldsymbol{u}_h - \boldsymbol{\pi}_h^0 \boldsymbol{u}\|$	EOC
$(\mu, \lambda) = (1, 1)$					
144	3680	3.82e+00	–	2.08e-01	–
608	17856	1.96e+00	0.97	6.97e-02	1.58
2496	78080	9.64e-01	1.02	1.87e-02	1.90
10112	326016	4.84e-01	1.00	4.74e-03	1.98
40704	1331840	2.43e-01	1.00	1.19e-03	1.99
$(\mu, \lambda) = (1, 1{,}000)$					
144	3680	5.09e+00	–	2.05e-01	–
608	17856	1.95e+00	1.38	7.15e-02	1.52
2496	78080	9.15e-01	1.09	2.00e-02	1.84
10112	326016	4.52e-01	1.02	5.18e-03	1.95
40704	1331840	2.25e-01	1.00	1.31e-03	1.98
$(\mu, \lambda) = (1, 1 \cdot 10^6)$					
144	3680	1.10e+02	–	2.05e-01	–
608	17856	1.48e+01	2.90	7.15e-02	1.52
2496	78080	2.07e+00	2.83	2.00e-02	1.84
10112	326016	5.08e-01	2.03	5.19e-03	1.95
40704	1331840	2.27e-01	1.16	1.31e-03	1.98

The corresponding forcing term is

$$\boldsymbol{f}(\boldsymbol{x}) = \mu \begin{pmatrix} 2\sin(\pi x_1)\sin(\pi x_2)\sin(\pi x_3) - \sin(\pi x_2)\cos(\pi(x_3+x_1)) - \sin(\pi x_3)\cos(\pi(x_1+x_2)) \\ 2\sin(\pi x_1)\sin(\pi x_2)\sin(\pi x_3) - \sin(\pi x_3)\cos(\pi(x_1+x_2)) - \sin(\pi x_1)\cos(\pi(x_2+x_3)) \\ 2\sin(\pi x_1)\sin(\pi x_2)\sin(\pi x_3) - \sin(\pi x_1)\cos(\pi(x_2+x_3)) - \sin(\pi x_2)\cos(\pi(x_3+x_1)) \end{pmatrix}$$
$$+ \lambda \begin{pmatrix} \sin(\pi x_1)\sin(\pi x_2)\sin(\pi x_3) - \cos(\pi x_1)\sin(\pi(x_2+x_3)) \\ \sin(\pi x_1)\sin(\pi x_2)\sin(\pi x_3) - \cos(\pi x_2)\sin(\pi(x_3+x_1)) \\ \sin(\pi x_1)\sin(\pi x_2)\sin(\pi x_3) - \cos(\pi x_3)\sin(\pi(x_1+x_2)) \end{pmatrix}.$$

For the numerical solution, we take $\mu = \lambda = 1$. Tables 6 and 7 collect the numerical results on, respectively Cartesian orthogonal and unstructured simplicial mesh families and pyramidal and prismatic mesh families. The monitored quantities are the same as for the other test cases. For the Cartesian orthogonal and simplicial meshes we add, for the sake of comparison, the number of unknowns and of nonzero matrix entries for the method of Di Pietro and Ern (2015) with $k = 1$. For all the mesh families, the asymptotic EOC for both the energy- and the L^2-norms of the error agree with the ones predicted. On the simplicial mesh family, an EOC close to 1 is attained starting from the third mesh refinement in the energy norm, whereas an EOC close to 2 is already observed starting from the second mesh refinement; on the other mesh families, the orders of convergence take a bit longer to settle to the corresponding asymptotic values, likely because the first computational meshes are coarser than in the simplicial case.

7. Local balances and continuity of numerical tractions

In this section we show that our method satisfies local force balances with equilibrated face tractions. This property can be exploited, e.g., to derive a posteriori error estimates by flux equilibration, and it makes the proposed method suitable for integration into existing Finite Volume codes.

Lemma 15 (Traction formulation of the discrete bilinear form)**.** *We have the following reformulation of the discrete*

Table 2
Numerical results for the test of Section 6.1, unstructured triangular mesh family.

$N_{\mathrm{dofs},h}$	$N_{\mathrm{nz},h}$	$\|\underline{\boldsymbol{u}}_h - \underline{\boldsymbol{I}}_h \boldsymbol{u}\|_{\mathrm{a},h}$	EOC	$\|\boldsymbol{u}_h - \boldsymbol{\pi}_h^0 \boldsymbol{u}\|$	EOC
$(\mu, \lambda) = (1, 1)$					
234	6572	3.00e+00	–	1.38e-01	–
978	30012	1.60e+00	0.90	4.11e-02	1.75
3986	127372	8.15e-01	0.98	9.37e-03	2.13
15542	505828	4.27e-01	0.93	2.61e-03	1.85
63584	2089920	2.12e-01	1.01	6.65e-04	1.97
249238	8228988	1.08e-01	0.97	1.71e-04	1.96
$(\mu, \lambda) = (1, 1{,}000)$					
234	6572	3.57e+00	–	1.45e-01	–
978	30012	1.60e+00	1.15	4.52e-02	1.68
3986	127372	8.00e-01	1.00	1.07e-02	2.07
15542	505828	4.18e-01	0.94	2.99e-03	1.85
63584	2089920	2.08e-01	1.01	7.63e-04	1.97
249238	8228988	1.06e-01	0.97	1.97e-04	1.96
$(\mu, \lambda) = (1, 1 \cdot 10^6)$					
234	6572	6.17e+01	–	1.45e-01	–
978	30012	7.55e+00	3.03	4.52e-02	1.68
3986	127372	1.14e+00	2.72	1.07e-02	2.07
15542	505828	4.33e-01	1.40	2.99e-03	1.85
63584	2089920	2.08e-01	1.06	7.63e-04	1.97
249238	8228988	1.06e-01	0.98	1.97e-04	1.96

bilinear form a_h *defined by* (22)*: For all* $\underline{\boldsymbol{w}}_h, \underline{\boldsymbol{v}}_h \in \underline{\boldsymbol{U}}_{h,0}$,

$$\mathrm{a}_h(\underline{\boldsymbol{w}}_h, \underline{\boldsymbol{v}}_h) = \sum_{T\in\mathcal{T}_h} \sum_{F\in\mathcal{F}_T} |F| \boldsymbol{\Phi}_{TF}(\underline{\boldsymbol{w}}_h)\cdot(\boldsymbol{v}_T - \boldsymbol{v}_F), \tag{56}$$

where, for all $T \in \mathcal{T}_h$ *and all* $F \in \mathcal{F}_T$*, we have introduced the numerical traction* $\boldsymbol{\Phi}_{TF} : \underline{\boldsymbol{U}}_T \to \mathbb{P}^0(F;\mathbb{R}^d)$ *such that*

$$\boldsymbol{\Phi}_{TF}(\underline{\boldsymbol{w}}_h) \coloneqq -\boldsymbol{\sigma}(\boldsymbol{\nabla}_{\mathrm{s}} p_T^1 \underline{\boldsymbol{w}}_T)\boldsymbol{n}_{TF} + (2\mu)\, \boldsymbol{\Phi}_{\mathrm{j},TF}(\underline{\boldsymbol{w}}_h) + (2\mu)\, \boldsymbol{\Phi}_{\mathrm{s},TF}(\underline{\boldsymbol{w}}_T),$$

with jump penalisation and stabilisation contributions respectively defined as

$$\boldsymbol{\Phi}_{\mathrm{j},TF}(\underline{\boldsymbol{w}}_h) \coloneqq \frac{\epsilon_{TF}}{h_F|F|}\int_F [p_h^1 \underline{\boldsymbol{w}}_h]_F + \sum_{G\in\mathcal{F}_T} \frac{\epsilon_{TG}}{h_G|T|}(\overline{\boldsymbol{x}}_G - \overline{\boldsymbol{x}}_T)\cdot\boldsymbol{n}_{TG}\int_G [p_h^1 \underline{\boldsymbol{w}}_h]_G,$$

$$\boldsymbol{\Phi}_{\mathrm{s},TF}(\underline{\boldsymbol{w}}_T) \coloneqq \frac{1}{h_F}\boldsymbol{\delta}_{TF}\underline{\boldsymbol{w}}_T + \sum_{G\in\mathcal{F}_T} \frac{|G|}{h_G|T|}(\overline{\boldsymbol{x}}_T - \overline{\boldsymbol{x}}_G)\cdot\boldsymbol{n}_{TF}\, \boldsymbol{\delta}_{TG}\underline{\boldsymbol{w}}_T,$$

where, for any X *mesh element or face, we have denoted by* $\overline{\boldsymbol{x}}_X \coloneqq \frac{1}{|X|}\int_X \boldsymbol{x}$ *its centroid and, for any* $T \in \mathcal{T}_h$ *and any* $F \in \mathcal{F}_T$, $\epsilon_{TF} \coloneqq \boldsymbol{n}_{TF}\cdot\boldsymbol{n}_F$ *defines the orientation of* F *relative to* T.

Proof. We proceed to reformulate the three terms in the right-hand side of (22) in order to highlight the corresponding

Table 3
Numerical results for the test of Section 6.1, Cartesian orthogonal mesh family.

$N_{\mathrm{dofs},h}$	$N_{\mathrm{nz},h}$	$\|\underline{\boldsymbol{u}}_h - \underline{\boldsymbol{I}}_h \boldsymbol{u}\|_{\mathrm{a},h}$	EOC	$\|\boldsymbol{u}_h - \boldsymbol{\pi}_h^0 \boldsymbol{u}\|$	EOC
$(\mu, \lambda) = (1, 1)$					
80	2768	3.13e+00	–	1.55e-01	–
352	15856	1.84e+00	0.77	4.08e-02	1.93
1472	73904	1.09e+00	0.75	1.04e-02	1.98
6016	317488	5.89e-01	0.89	2.89e-03	1.84
24320	1314608	3.02e-01	0.97	7.73e-04	1.90
$(\mu, \lambda) = (1, 1{,}000)$					
80	2768	3.08e+00	–	1.64e-01	–
352	15856	1.81e+00	0.77	4.72e-02	1.80
1472	73904	1.08e+00	0.75	1.37e-02	1.78
6016	317488	5.81e-01	0.89	3.96e-03	1.79
24320	1314608	2.97e-01	0.97	1.06e-03	1.90
$(\mu, \lambda) = (1, 1 \cdot 10^6)$					
80	2768	3.08e+00	–	1.64e-01	–
352	15856	1.81e+00	0.77	4.72e-02	1.80
1472	73904	1.08e+00	0.75	1.37e-02	1.78
6016	317488	5.81e-01	0.89	3.96e-03	1.79
24320	1314608	2.97e-01	0.97	1.06e-03	1.90

contribution to the numerical traction. For the consistency term, we can write

$$\begin{aligned}(\boldsymbol{\sigma}(\boldsymbol{\nabla}_{\mathrm{s},h} p_h^1 \underline{\boldsymbol{w}}_h), \boldsymbol{\nabla}_{\mathrm{s},h} p_h^1 \underline{\boldsymbol{v}}_h) &= \sum_{T\in\mathcal{T}_h} |T| \boldsymbol{\sigma}(\boldsymbol{\nabla}_{\mathrm{s}} p_T^1 \underline{\boldsymbol{w}}_T) : \boldsymbol{\nabla}_{\mathrm{s}} p_T^1 \underline{\boldsymbol{v}}_T = \sum_{T\in\mathcal{T}_h} |T| \boldsymbol{\sigma}(\boldsymbol{\nabla}_{\mathrm{s}} p_T^1 \underline{\boldsymbol{w}}_T) : \boldsymbol{\nabla} p_T^1 \underline{\boldsymbol{v}}_T \\ &= \sum_{T\in\mathcal{T}_h} |T| \boldsymbol{\sigma}(\boldsymbol{\nabla}_{\mathrm{s}} p_T^1 \underline{\boldsymbol{w}}_T) : \left(\sum_{F\in\mathcal{F}_T} \frac{|F|}{|T|} (\boldsymbol{v}_F - \boldsymbol{v}_T) \otimes \boldsymbol{n}_{TF} \right) \\ &= - \sum_{T\in\mathcal{T}_h} \sum_{F\in\mathcal{F}_T} |F| \boldsymbol{\sigma}(\boldsymbol{\nabla}_{\mathrm{s}} p_T^1 \underline{\boldsymbol{w}}_T) \boldsymbol{n}_{TF} \cdot (\boldsymbol{v}_T - \boldsymbol{v}_F),\end{aligned}$$

where we have used the fact that, for any $T \in \mathcal{T}_h$, both $\boldsymbol{\sigma}(\boldsymbol{\nabla}_{\mathrm{s}} p_T^1 \underline{\boldsymbol{w}}_T)$ and $\boldsymbol{\nabla}_{\mathrm{s}} p_T^1 \underline{\boldsymbol{v}}_T$ are constant inside T along with the fact that $\boldsymbol{\sigma}(\boldsymbol{\nabla}_{\mathrm{s}} p_T^1 \underline{\boldsymbol{w}}_T)$ is symmetric to replace $\boldsymbol{\nabla}_{\mathrm{s}}$ with $\boldsymbol{\nabla}$ in the first line, the first relation in (18) to pass to the second line, and we have rearranged the products and sums to conclude.

For the jump penalisation term, we can start by observing that

$$\begin{aligned}\mathrm{j}_h(\underline{\boldsymbol{w}}_h, \underline{\boldsymbol{v}}_h) &= \sum_{F\in\mathcal{F}_h} \frac{1}{h_F} \left([p_h^1 \underline{\boldsymbol{w}}_h]_F, [p_h^1 \underline{\boldsymbol{v}}_h]_F \right)_F \\ &= \sum_{F\in\mathcal{F}_h} \sum_{T\in\mathcal{F}_F} \frac{\epsilon_{TF}}{h_F} \left([p_h^1 \underline{\boldsymbol{w}}_h]_F, p_T^1 \underline{\boldsymbol{v}}_T \right)_F = \sum_{T\in\mathcal{T}_h} \sum_{F\in\mathcal{F}_T} \frac{\epsilon_{TF}}{h_F} \left([p_h^1 \underline{\boldsymbol{w}}_h]_F, p_T^1 \underline{\boldsymbol{v}}_T \right)_F,\end{aligned}$$

where we have used the definition of the jump operator to pass to the second line and exchanged the sums over elements and faces according to (39) to conclude.

Table 4
Numerical results for the test of Section 6.1, distorted quadrangular mesh family.

$N_{\mathrm{dofs},h}$	$N_{\mathrm{nz},h}$	$\|\|\underline{\boldsymbol{u}}_h - \underline{\boldsymbol{I}}_h \boldsymbol{u}\|\|_{\mathrm{a},h}$	EOC	$\|\|\boldsymbol{u}_h - \boldsymbol{\pi}_h^0 \boldsymbol{u}\|\|$	EOC
$(\mu, \lambda) = (1, 1)$					
80	2768	3.51e+00	–	1.89e-01	–
352	15856	1.91e+00	0.88	5.45e-02	1.79
1472	73904	1.08e+00	0.82	1.34e-02	2.03
6016	317488	5.83e-01	0.89	3.52e-03	1.93
24320	1314608	2.97e-01	0.97	9.18e-04	1.94
97792	5348656	1.49e-01	0.99	2.33e-04	1.98
$(\mu, \lambda) = (1, 1{,}000)$					
80	2768	3.44e+00	–	1.96e-01	–
352	15856	1.87e+00	0.88	5.89e-02	1.73
1472	73904	1.07e+00	0.81	1.63e-02	1.85
6016	317488	5.74e-01	0.89	4.48e-03	1.86
24320	1314608	2.92e-01	0.97	1.18e-03	1.93
97792	5348656	1.47e-01	0.99	3.00e-04	1.97
$(\mu, \lambda) = (1, 1 \cdot 10^6)$					
80	2768	9.12e+00	–	1.96e-01	–
352	15856	2.27e+00	2.00	5.89e-02	1.73
1472	73904	1.08e+00	1.07	1.63e-02	1.85
6016	317488	5.74e-01	0.91	4.48e-03	1.86
24320	1314608	2.92e-01	0.97	1.18e-03	1.93
97792	5348656	1.47e-01	0.99	3.00e-04	1.97

Table 5
Numerical results for the test of Section 6.2 and comparison with the high-order method of Di Pietro and Ern (2015) with $k = 1$. For the latter, the energy norm is the one associated to the corresponding bilinear form without jump stabilisation.

$N_{\mathrm{dofs},h}$	$N_{\mathrm{nz},h}$	$\|\|\underline{\boldsymbol{u}}_h - \underline{\boldsymbol{I}}_h \boldsymbol{u}\|\|_{\mathrm{a},h}$	EOC	$\|\|\boldsymbol{u}_h - \boldsymbol{\pi}_h^0 \boldsymbol{u}\|\|$	EOC
Present work					
256	10616	7.65e-01	–	7.51e-02	–
1088	52728	5.63e-01	0.44	3.34e-02	1.17
4480	232568	3.97e-01	0.50	1.40e-02	1.25
18176	974712	2.76e-01	0.53	5.72e-03	1.29
73216	3988856	1.90e-01	0.54	2.31e-03	1.31
293888	16136568	1.31e-01	0.54	9.29e-04	1.31
HHO method of Di Pietro and Ern (2015), $k = 1$					
320	7584	1.07e-01	–	9.40e-03	–
1408	36512	7.32e-02	0.55	3.64e-03	1.37
5888	158880	5.01e-02	0.55	1.41e-03	1.36
24064	661664	3.43e-02	0.55	5.52e-04	1.36
97280	2699424	2.35e-02	0.54	2.17e-04	1.35
391168	10903712	1.61e-02	0.54	8.57e-05	1.34

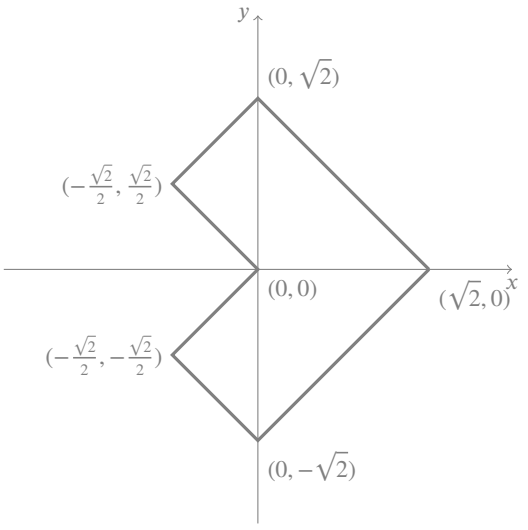

Figure 3: Domain for the test case of Section 6.2.

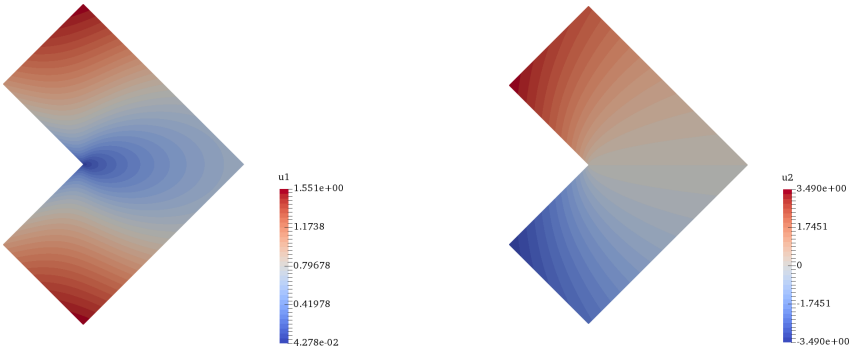

(a) u_1 (b) u_2

Figure 4: Numerical solution for the test of Section 6.2.

Using the explicit expression (19) of the local displacement reconstruction, we can go on writing

$$
\begin{aligned}
\mathrm{j}_h(\underline{\boldsymbol{w}}_h, \underline{\boldsymbol{v}}_h) &= \sum_{T\in\mathcal{T}_h}\sum_{F\in\mathcal{F}_T} \frac{\epsilon_{TF}}{h_F}\left([\boldsymbol{p}_h^1\underline{\boldsymbol{w}}_h]_F, \boldsymbol{v}_T + \sum_{G\in\mathcal{F}_T}\frac{|G|}{|T|}(\boldsymbol{x}-\overline{\boldsymbol{x}}_T)\cdot\boldsymbol{n}_{TF}(\boldsymbol{v}_G-\boldsymbol{v}_T)\right)_F\\
&= \sum_{T\in\mathcal{T}_h}\sum_{F\in\mathcal{F}_T} \frac{\epsilon_{TF}}{h_F}\left([\boldsymbol{p}_h^1\underline{\boldsymbol{w}}_h]_F, \boldsymbol{v}_T-\boldsymbol{v}_F\right)_F\\
&\quad + \sum_{T\in\mathcal{T}_h}\sum_{F\in\mathcal{F}_T}\sum_{G\in\mathcal{F}_T} \frac{\epsilon_{TF}|G|}{h_F|T|}\left([\boldsymbol{p}_h^1\underline{\boldsymbol{w}}_h]_F(\boldsymbol{x}-\overline{\boldsymbol{x}}_T)\cdot\boldsymbol{n}_{TF}, \boldsymbol{v}_G-\boldsymbol{v}_T\right)_F\\
&= \sum_{T\in\mathcal{T}_h}\sum_{F\in\mathcal{F}_T} |F|\left(\frac{\epsilon_{TF}}{h_F|F|}\int_F [\boldsymbol{p}_h^1\underline{\boldsymbol{w}}_h]_F\right)\cdot(\boldsymbol{v}_T-\boldsymbol{v}_F)\\
&\quad - \sum_{T\in\mathcal{T}_h}\sum_{G\in\mathcal{F}_T} |G|\left(\sum_{F\in\mathcal{F}_T}\frac{\epsilon_{TF}}{h_F|T|}\int_F [\boldsymbol{p}_h^1\underline{\boldsymbol{w}}_h]_F(\boldsymbol{x}-\overline{\boldsymbol{x}}_T)\cdot\boldsymbol{n}_{TF}\right)\cdot(\boldsymbol{v}_T-\boldsymbol{v}_G)\\
&= \sum_{T\in\mathcal{T}_h}\sum_{F\in\mathcal{F}_T} |F|\boldsymbol{\Phi}_{\mathrm{j},TF}(\underline{\boldsymbol{w}}_h)\cdot(\boldsymbol{v}_T-\boldsymbol{v}_F),
\end{aligned}
$$

Table 6
Numerical results for the test of Section 6.3 on Carthesian orthogonal and simplicial meshes. The number of degrees of freedom and of nonzero matrix entries for the method of Di Pietro and Ern (2015) are also included for comparison (except for the last mesh refinement).

$N_{\mathrm{dofs},h}$		$N_{\mathrm{nz},h}$		$\|\underline{\boldsymbol{u}}_h - \underline{\boldsymbol{I}}_h \boldsymbol{u}\|_{\mathrm{a},h}$	EOC	$\|\boldsymbol{u}_h - \boldsymbol{\pi}_h^0 \boldsymbol{u}\|$	EOC
$k=0$	$(k=1)$	$k=0$	$(k=1)$				
Cartesian orthogonal mesh sequence							
624	(1296)	70128	(97200)	2.07e+00	–	1.01e-01	–
5568	(12096)	831024	(1057536)	1.31e+00	0.65	4.09e-02	1.30
46848	(103680)	7879824	(9673344)	7.19e-01	0.87	1.27e-02	1.68
384000	(857088)	68277456	(82425600)	3.71e-01	0.95	3.46e-03	1.88
3108864	–	567808848	–	1.87e-01	0.98	8.95e-04	1.95
Unstructured simplicial mesh sequence							
1584	(3024)	107136	(167184)	1.38e+00	–	4.70e-02	–
13248	(25920)	1008288	(1539648)	7.61e-01	0.85	1.64e-02	1.52
108288	(214272)	8676288	(13125888)	3.96e-01	0.94	4.39e-03	1.91
875520	(1741824)	71860608	(108241920)	2.02e-01	0.97	1.14e-03	1.95
7041024	–	584706816	–	1.02e-01	0.99	2.89e-04	1.98

Table 7
Numerical results for the test of Section 6.3 on pyramidal and prismatic mesh sequences.

$N_{\mathrm{dofs},h}$	$N_{\mathrm{nz},h}$	$\|\underline{\boldsymbol{u}}_h - \underline{\boldsymbol{I}}_h \boldsymbol{u}\|_{\mathrm{a},h}$	EOC	$\|\boldsymbol{u}_h - \boldsymbol{\pi}_h^0 \boldsymbol{u}\|$	EOC
Pyramidal mesh sequence					
468	36180	1.91e+00	–	7.87e-02	–
3888	345168	1.18e+00	0.70	3.34e-02	1.23
31680	2989440	6.32e-01	0.90	1.01e-02	1.73
255744	24838272	3.23e-01	0.97	2.69e-03	1.90
2055168	202417920	1.63e-01	0.99	6.91e-04	1.96
Prismatic mesh sequence					
120	6192	2.29e+00	–	1.20e-01	–
1152	103464	1.74e+00	0.39	6.52e-02	0.89
9984	1098792	1.01e+00	0.79	2.35e-02	1.47
82944	9980712	5.28e-01	0.93	6.83e-03	1.78
675840	84823848	2.68e-01	0.98	1.81e-03	1.92

where, to insert $\boldsymbol{v}_F$ into the first term in the second line, we have used the fact that $[\boldsymbol{p}_h^1 \underline{\boldsymbol{w}}_h]_F$ is single-valued at interfaces together with $\boldsymbol{v}_F = \boldsymbol{0}$ on boundary faces, to pass to the third line we have used the fact that the discrete unknowns in $\underline{\boldsymbol{v}}_h$ are constant over mesh elements to take them out of the integrals over faces while, to conclude, we have observed that $(\boldsymbol{x} - \overline{\boldsymbol{x}}_T)\cdot\boldsymbol{n}_{TF} = (\overline{\boldsymbol{x}}_F - \overline{\boldsymbol{x}}_T)\cdot\boldsymbol{n}_{TF}$ for all $\boldsymbol{x} \in F$ and we have used the definition of $\boldsymbol{\Phi}_{\mathrm{j},TF}(\underline{\boldsymbol{w}}_h)$ after switching the names of the mute variables F and G in the second term of the third line.

Moving to the stabilisation term, we can write

$$\begin{aligned}
\mathrm{s}_h(\underline{\boldsymbol{w}}_h,\underline{\boldsymbol{v}}_h) &= \sum_{T\in\mathcal{T}_h}\sum_{F\in\mathcal{F}_T}\frac{|F|}{h_F}\boldsymbol{\delta}_{TF}\underline{\boldsymbol{w}}_T\cdot\boldsymbol{\delta}_{TF}\underline{\boldsymbol{v}}_T\\
&= \sum_{T\in\mathcal{T}_h}\sum_{F\in\mathcal{F}_T}\frac{|F|}{h_F}\boldsymbol{\delta}_{TF}\underline{\boldsymbol{w}}_T\cdot\left(\boldsymbol{v}_T-\boldsymbol{v}_F+\sum_{G\in\mathcal{F}_T}\frac{|G|}{|T|}(\boldsymbol{v}_G-\boldsymbol{v}_T)(\overline{\boldsymbol{x}}_F-\overline{\boldsymbol{x}}_T)\cdot\boldsymbol{n}_{TG}\right)\\
&= \sum_{T\in\mathcal{T}_h}\sum_{F\in\mathcal{F}_T}\frac{|F|}{h_F}\boldsymbol{\delta}_{TF}\underline{\boldsymbol{w}}_T\cdot(\boldsymbol{v}_T-\boldsymbol{v}_F)\\
&\quad+\sum_{T\in\mathcal{T}_h}\sum_{G\in\mathcal{F}_T}|G|\left(\sum_{F\in\mathcal{F}_T}\frac{|F|}{h_F|T|}(\overline{\boldsymbol{x}}_T-\overline{\boldsymbol{x}}_F)\cdot\boldsymbol{n}_{TG}\,\boldsymbol{\delta}_{TF}\underline{\boldsymbol{w}}_T\right)\cdot(\boldsymbol{v}_T-\boldsymbol{v}_G)\\
&= \sum_{T\in\mathcal{T}_h}\sum_{F\in\mathcal{F}_T}|F|\boldsymbol{\Phi}_{\mathrm{s},TF}(\underline{\boldsymbol{w}}_T)\cdot(\boldsymbol{v}_T-\boldsymbol{v}_F),
\end{aligned}$$

where we have used the definition (24) of the boundary difference operator together with the explicit expression (19) of the local displacement reconstruction to pass to the second line, we have rearranged the terms to pass to the third line, and we have used the definition of $\boldsymbol{\Phi}_{\mathrm{s},TF}(\underline{\boldsymbol{w}}_T)$ after switching the names of the mute variables F and G in the second term of the third line to conclude. □

Corollary 16 (Local balances and equilibrated tractions)**.** *Under the assumptions and notations of Lemma 15, we have that $\underline{\boldsymbol{u}}_h\in\underline{\boldsymbol{U}}_{h,0}$ solves the discrete problem (32) if and only if: For all $T\in\mathcal{T}_h$ the following balance holds*

$$\sum_{F\in\mathcal{F}_T}|F|\boldsymbol{\Phi}_{TF}(\underline{\boldsymbol{u}}_h)=\int_T\boldsymbol{f},\tag{57}$$

and, for any interface $F\in\mathcal{F}_h^{\mathrm{i}}$ shared by the mesh elements T_1 and T_2, it holds that

$$\boldsymbol{\Phi}_{T_1F}(\underline{\boldsymbol{u}}_h)+\boldsymbol{\Phi}_{T_2F}(\underline{\boldsymbol{u}}_h)=\boldsymbol{0}.\tag{58}$$

Proof. Plugging the flux reformulation (56) of the bilinear form a_h into the discrete problem (32), and recalling (16), we infer that it is equivalent to: Find $\underline{\boldsymbol{u}}_h\in\underline{\boldsymbol{U}}_{h,0}$ such that

$$\sum_{T\in\mathcal{T}_h}\sum_{F\in\mathcal{F}_T}|F|\boldsymbol{\Phi}_{TF}(\underline{\boldsymbol{u}}_h)\cdot(\boldsymbol{v}_T-\boldsymbol{v}_F)=\sum_{T\in\mathcal{T}_h}\int_T\boldsymbol{f}\cdot\boldsymbol{v}_T\qquad\forall\underline{\boldsymbol{v}}_h\in\underline{\boldsymbol{U}}_{h,0}.\tag{59}$$

Taking, for a given mesh element $T\in\mathcal{T}_h$, $\underline{\boldsymbol{v}}_h$ such that $\boldsymbol{v}_{T'}=\boldsymbol{0}$ for all $T'\in\mathcal{T}_h\setminus\{T\}$, $\boldsymbol{v}_F=\boldsymbol{0}$ for all $F\in\mathcal{F}_h$, and letting $\boldsymbol{v}_T$ span $\mathbb{P}^0(T;\mathbb{R}^d)$, (59) reduces to (57). Similarly, given an interface $F\in\mathcal{F}_h^{\mathrm{i}}$ shared by the mesh elements T_1 and T_2, taking in (59) $\underline{\boldsymbol{v}}_h$ such that $\boldsymbol{v}_T=\boldsymbol{0}$ for all $T\in\mathcal{T}_h$, $\boldsymbol{v}_{F'}=\boldsymbol{0}$ for all $F'\in\mathcal{F}_h\setminus\{F\}$, and letting $\boldsymbol{v}_F$ span $\mathbb{P}^0(F;\mathbb{R}^d)$, (59) reduces to (58) after recalling that the numerical tractions are constant over F. □

References

Ainsworth, M., Senior, B., 1997. Aspects of an adaptive hp-finite element method: Adaptive strategy, conforming approximation and efficient solvers. Comput. Meth. Appl. Mech. Engrg. 150, 65–87. doi:S0045782597001011.

Amrouche, C., Girault, V., 1991. On the existence and regularity of the solution of Stokes problem in arbitrary dimension. Proc. Japan. Acad. 67, 171–175.

Artioli, E., Beirão da Veiga, L., Lovadina, C., Sacco, E., 2017. Arbitrary order 2D virtual elements for polygonal meshes: part I, elastic problem. Comput. Mech. 60, 355–377. doi:10.1007/s00466-017-1404-5.

Beirão da Veiga, L., Brezzi, F., Marini, L.D., 2013. Virtual elements for linear elasticity problems. SIAM J. Numer. Anal. 2, 794–812. doi:10.1142/S0218202512500492.

Botti, M., Di Pietro, D.A., Sochala, P., 2017. A Hybrid High-Order method for nonlinear elasticity. SIAM J. Numer. Anal. 55, 2687–2717. doi:10.1137/16M1105943.

Brenner, S.C., 1993. A nonconforming mixed multigrid method for the pure displacement problem in planar linear elasticity. SIAM J. Numer. Anal. 30, 116–135. doi:10.1137/0730006.

Brenner, S.C., 2003. Poincaré-Friedrichs inequalities for piecewise H^1 functions. SIAM J. Numer. Anal. 41, 306–324. doi:10.1137/S0036142902401311.

Brenner, S.C., Sung, L.Y., 1992. Linear finite element methods for planar linear elasticity. Math. Comp. 59, 321–338. doi:10.2307/2153060.

Cáceres, E., Gatica, G.N., Sequeira, F.A., 2019. A mixed virtual element method for a pseudostress-based formulation of linear elasticity. Appl. Numer. Math. 135, 423–442. doi:10.1016/j.apnum.2018.09.003.

Cangiani, A., Dong, Z., Georgoulis, E.H., Houston, P., 2017. *hp*-version discontinuous Galerkin methods on polygonal and polyhedral meshes. SpringerBriefs in Mathematics, Springer, Cham.

Cockburn, B., Fu, G., 2018. Devising superconvergent HDG methods with symmetric approximate stresses for linear elasticity by M-decompositions. IMA J. Numer. Anal. 38, 566–604. doi:10.1093/imanum/drx025.

Beirão Da Veiga, L., 2010. A mimetic discretization method for linear elasticity. M2AN Math. Model. Numer. Anal. 44, 231–250. doi:10.1051/m2an/2010001.

Di Pietro, D.A., Droniou, J., 2017a. A Hybrid High-Order method for Leray–Lions elliptic equations on general meshes. Math. Comp. 86, 2159–2191. doi:10.1090/mcom/3180.

Di Pietro, D.A., Droniou, J., 2017b. $W^{s,p}$-approximation properties of elliptic projectors on polynomial spaces, with application to the error analysis of a Hybrid High-Order discretisation of Leray–Lions problems. Math. Models Methods Appl. Sci. 27, 879–908. doi:10.1142/S0218202517500191.

Di Pietro, D.A., Droniou, J., 2018. A third Strang lemma for schemes in fully discrete formulation. Calcolo 55. doi:10.1007/s10092-018-0282-3.

Di Pietro, D.A., Droniou, J., 2019. The hybrid high-order method for polytopal meshes — design, analysis and applications. Submitted.

Di Pietro, D.A., Ern, A., 2010. Discrete functional analysis tools for discontinuous Galerkin methods with application to the incompressible Navier-Stokes equations. Math. Comp. 79, 1303–1330. doi:10.1090/S0025-5718-10-02333-1.

Di Pietro, D.A., Ern, A., 2012. Mathematical aspects of discontinuous Galerkin methods. volume 69 of *Mathématiques & Applications (Berlin) [Mathematics & Applications]*. Springer, Heidelberg. doi:10.1007/978-3-642-22980-0.

Di Pietro, D.A., Ern, A., 2015. A hybrid high-order locking-free method for linear elasticity on general meshes. Comput. Meth. Appl. Mech. Engrg. 283, 1–21. doi:10.1016/j.cma.2014.09.009.

Di Pietro, D.A., Ern, A., Lemaire, S., 2014. An arbitrary-order and compact-stencil discretization of diffusion on general meshes based on local reconstruction operators. Comput. Meth. Appl. Math. 14, 461–472. doi:10.1515/cmam-2014-0018.

Di Pietro, D.A., Lemaire, S., 2015. An extension of the Crouzeix–Raviart space to general meshes with application to quasi-incompressible linear elasticity and Stokes flow. Math. Comp. 84, 1–31. doi:10.1090/S0025-5718-2014-02861-5.

Di Pietro, D.A., Tittarelli, R., 2018. Numerical Methods for PDEs. Springer. chapter An introduction to Hybrid High-Order methods. 15. doi:10.1007/978-3-319-94676-4. SEMA-SIMAI.

Droniou, J., Eymard, R., Gallouët, T., Guichard, C., Herbin, R., 2018. The gradient discretisation method. volume 82 of *Mathematics & Applications*. Springer. doi:10.1007/978-3-319-79042-8.

Droniou, J., Lamichhane, B.P., 2015. Gradient schemes for linear and non-linear elasticity equations. Numer. Math. 129, 251–277. doi:10.1007/s00211-014-0636-y.

Gain, A.L., Talischi, C., Paulino, G.H., 2014. On the virtual element method for three-dimensional linear elasticity problems on arbitrary polyhedral meshes. Comput. Methods Appl. Mech. Engrg. 282, 132–160. doi:10.1016/j.cma.2014.05.005.

Hansbo, P., Larson, M.G., 2003. Discontinuous Galerkin and the Crouzeix-Raviart element: application to elasticity. M2AN Math. Model. Numer. Anal. 37, 63–72. doi:10.1051/m2an:2003020.

Hughes, T.J.R., Cottrell, J.A., Bazilevs, Y., 2005. Isogeometric analysis: CAD, finite elements, NURBS, exact geometry and mesh refinement. Comput. Methods Appl. Mech. Engrg. 194, 4135–4195. doi:10.1016/j.cma.2004.10.008.

Karakashian, O.A., Pascal, F., 2003. A posteriori error estimates for a discontinuous Galerkin approximation of second-order elliptic problems. SIAM J. Numer. Anal. 41, 2374–2399. doi:10.1137/S0036142902405217.

Koyama, D., Kikuchi, F., 2017. On volumetric locking in a hybrid symmetric interior penalty method for nearly incompressible linear elasticity on polygonal meshes. Jpn. J. Ind. Appl. Math. 34, 373–406. doi:10.1007/s13160-017-0251-2.

Sevilla, R., Giacomini, M., Karkoulias, A., Huerta, A., 2018. A superconvergent hybridisable discontinuous Galerkin method for linear elasticity. Internat. J. Numer. Methods Engrg. 116, 91–116. doi:10.1002/nme.5916.

Tabarraei, A., Sukumar, N., 2006. Application of polygonal finite elements in linear elasticity. Int. J. Comput. Methods 3. doi:10.1142/S021987620600117X.

Wriggers, P., Rust, W.T., Reddy, B.D., 2016. A virtual element method for contact. Computational Mechanics 58, 1039–1050. doi:10.1007/s00466-016-1331-x.